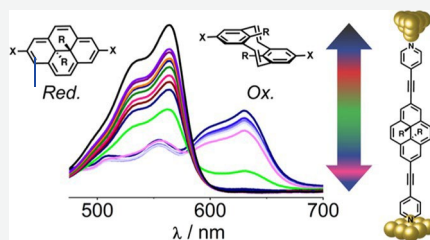


2,7- and 4,9-Dialkynyldihdropyrene Molecular Switches: Syntheses, Properties, and Charge Transport in Single-Molecule Junctions

Max Roemer, Angus Gillespie, David Jago, David Costa-Milan, Jehan Alqahtani, Juan Hurtado-Gallego, Hatef Sadeghi, Colin J. Lambert, Peter R. Spackman, Alexandre N. Sobolev, Brian W. Skelton, Arnaud Grosjean, Mark Walkey, Sven Kampmann, Andrea Vezzoli, Peter V. Simpson, Massimiliano Massi, Inco Planje, Gabino Rubio-Bollinger, Nicolás Agraït, Simon J. Higgins, Sara Sangtarash, Matthew J. Piggott, Richard J. Nichols, and George A. Koutsantonis*

ABSTRACT: This paper describes the syntheses of several functionalized dihydropyrene (DHP) molecular switches with different substitution patterns. Regioselective nucleophilic alkylation of a 5-substituted dimethyl isophthalate allowed the development of a workable synthetic protocol for the preparation of 2,7-alkyne-functionalized DHPs. Synthesis of DHPs with surface-anchoring groups in the 2,7- and 4,9-positions is described. The molecular structures of several intermediates and DHPs were elucidated by X-ray single-crystal diffraction. Molecular properties and switching capabilities of both types of DHPs were assessed by light irradiation experiments, spectroelectrochemistry, and cyclic voltammetry. Spectroelectrochemistry, in combination with density functional theory (DFT) calculations, shows reversible electrochemical switching from the DHP forms to the cyclophanediene (CPD) forms. Charge-transport behavior was assessed in single-molecule scanning tunneling microscope (STM) break junctions, combined with density functional theory-based quantum transport calculations. All DHPs with surface-contacting groups form stable molecular junctions. Experiments show that the molecular conductance depends on the substitution pattern of the DHP motif. The conductance was found to decrease with increasing applied bias.



INTRODUCTION

The manipulation of charge transport through molecules defines the field of molecular electronics, which has a rich history.¹ This multidisciplinary field uses molecules, or arrays of molecules, to mimic the function of electronic devices, currently the exclusive domain of complementary metal–oxide–semiconductor (CMOS) components. Molecules are an attractive option to maintain the rate of miniaturization of electronic components and overcome the challenges of top-down nanofabrication. Additionally, measurements of the electrical properties of single-molecule junctions have also provided a wealth of information on molecular charge transport. Studies of single-molecule junctions have helped to understand the dependence of charge transport on molecular and electronic structure, molecular conformation, contacting electrode materials, bias voltage, electrochemical potential, and molecule–electrode interaction.^{2–4} These studies have contributed to the design and fabrication of junctions that are optimized in terms of stability, robustness, reproducibility, and of course function. The feasibility of such an endeavor has recently been investigated by incorporating molecular junctions as active components in audio clipping circuits.⁵

While architectures for electron transport through molecular wires are well developed,⁶ more functional electronic components such as molecular rectifiers (diodes) and molecular switches^{7,8} are subject to current efforts in the field. A rectifier is a two-terminal device in which current flow is permitted for a given polarity of the voltage applied across its termini but impeded when the polarity is reversed. Traditional electronics has relied on the applied bias, but memory elements are commonly addressed by magnetic or optical stimuli.² Various approaches have been used to mimic the rectification behavior with single molecules. Among the first ideas of theoretical nature was the Aviram–Ratner diode based on a donor–acceptor-type molecule.⁹ More recently, a number of molecular diodes, in either single-molecule devices^{10,11} or large-area ensemble devices have been fabricated.^{12–14} Switching is a particularly desirable function that involves reversible control of current flowing through a molecular junction using

an external stimulus.^{15–17} As an alternative to gating through conformational changes to the orientation of the phenylene ring systems in bis(thiolate)-contacted biphenyl-based molecular transistors,¹⁸ other topological switching moieties can be introduced into the conjugation pathway. Optoelectronic devices based on photochromic molecules are attractive for molecular electronic studies since fast controllable switching might ultimately be achievable. For example, the dithienylethene molecular switch is a popular motif for incorporation into nascent molecular components and memory applications.^{19–21}

Here, we consider structures shown in Figure 1 based on dihydropyrene (DHP) as precursors to switchable molecular components.

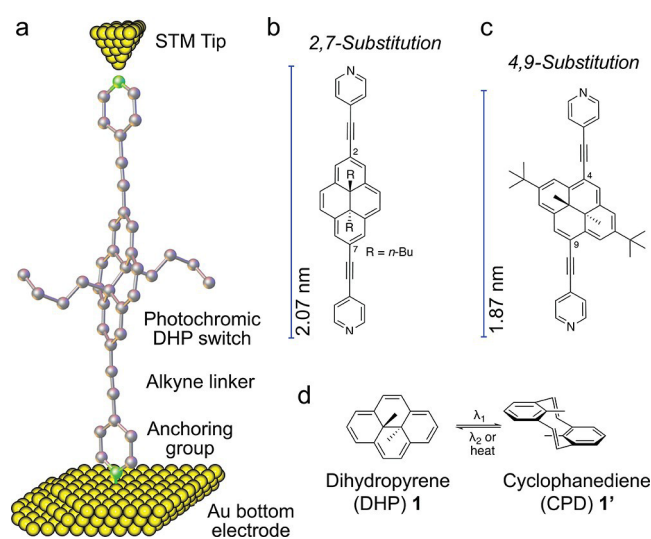


Figure 1. (a) Schematics of a single-molecule scanning tunneling microscope (STM) junction of a 2,7-substituted dihydropyrene sandwiched between two gold electrodes. (b, c) Different substitution patterns of the compounds studied herein and their molecular lengths. (d) *Trans*-10b,10c-dimethyl-10b,10c-dihydropyrene (1) and its cyclophanediene valence tautomer (1').

DHPs are photochromic molecules that can isomerize to the cyclophanediene (CPD) isomer 1' when irradiated with visible light. Back-conversion can be achieved by irradiation with UV light or heat. The colored DHP is significantly more conjugated than the colorless CPD isomer, which in turn results in DHP being more electrically conductive.^{22,23} This allows switching of electrical current by isomerization when incorporated into a molecular device.^{24–27}

With respect to molecular electronics applications, DHPs may offer advantages over dithienylethene-based components as there is less structural reorganization between the open 1' and closed 1 forms. In addition, there is greater scope for functionalization of DHPs when compared with the rather prescriptive structures necessary for efficient switching of dithienylethenes.^{24,28–30} With the appropriate internal substituents, thermal half-lives of the less-stable CPD isomer at 20 °C can be greater than 10 years, time frames compatible with long-term memory storage.³¹ A large number of DHPs, with varying degree of functionalization, have been reported, all of which require multistep synthetic procedures.^{31–39} Some systems are relatively straightforward to obtain with optimized protocols, such as 2,7-di-*tert*-butyl-*trans*-10b,10c-dimethyldihy-

dropyrene⁴⁰ (5, Scheme 1). The *tert*-butyl substituents assist both in the regioselective preparation of starting materials with appropriate substitution pattern (step a), and the macrocyclization (step b) involved in the synthesis of 5.⁴⁰

Due to its optimized large-scale synthesis,⁴⁰ 5 is perhaps the most studied and derivatized DHP. In contrast to their 4,9-substituted regioisomers, DHPs bearing 2,7-substituents other than *tert*-butyl are relatively rare and considerably more difficult to synthesize. Syntheses require many steps,^{41–43} overall yields are low, and the scope for late-stage diversification is limited. Possible strategies for the preparation of useful 2,7-disubstituted DHPs include regioselective functionalization of the parent DHP or application of established DHP synthetic routes to suitably substituted starting materials. We reasoned that 2,7-substitution with the appropriate internal substitution would provide good candidates for stable molecular electronic junctions as the number of binding configurations in the junction would be minimized. Larger internal substituents would result in the reduced probability of the molecule of interest lying flat down in the junction, with an anticipated higher probability of end-to-end binding through surface-anchoring groups. Molecular shape through substitution has been found to significantly affect the orientation of the molecule in metal/molecule/metal junctions.^{44,45}

Herein, we describe the synthesis of DHPs substituted with 2,7-ethynyl substituents, represented in Figure 1, enabled by the serendipitous discovery of a novel nucleophilic oxidative aromatic alkylation reaction. In addition, we report analogous 4,9-substituted DHPs for comparative characterization. We examined the charge-transport properties of both types of DHP motifs synthesized and their subsequent stability in those junctions. Spectroelectrochemical experiments, supported by DFT calculations, demonstrate electrochemical switching.

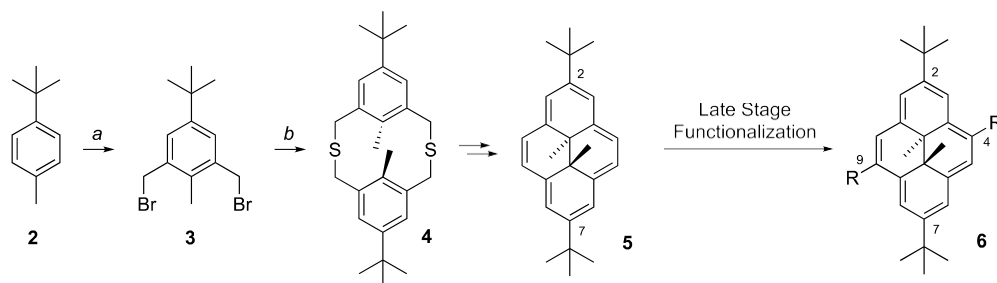
RESULTS AND DISCUSSION

Syntheses of 2,7-Functionalized DHPs. We developed a viable synthetic route to 2,7-diethynyl-DHPs starting from dimethyl 5-bromoisophthalate. The originally proposed route to 2,7-diethynyl-DHPs 12 is set out in Scheme 1. After Sonogashira coupling of commercially available dimethyl 5-bromoisophthalate with a protected acetylene, directed metalation of 7 to give 8 would be followed by a reaction with an electrophile to provide aryl halides 9. Further modification would allow installation of the substituent R in 10. Reduction and dehydroxyhalogenation would then provide key *m*-xylylene dihalides 11 necessary for macrocyclization toward the target DHPs 12.

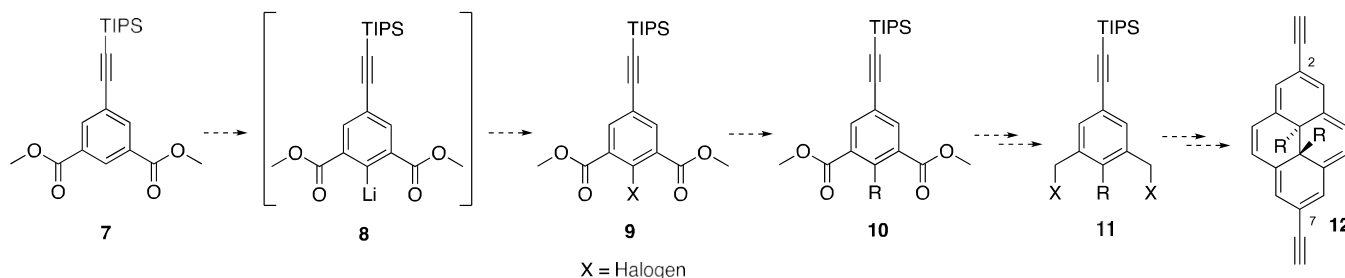
There is one report of the magnesiation of an isophthalate diester,⁴⁶ and the corresponding *sym*-diisopropylisophthalamide has been 2-lithiated.⁴⁷ Ethyl benzoate can also be *ortho*-lithiated at a low temperature with LiTMP and the aryllithium captured by electrophiles in high yield, leaving the ester functionality intact.⁴⁸ With these precedents in mind, the lithiation of the TIPS-protected isophthalate diester 7 was attempted with various bases, followed by quenching with iodine (Scheme 2). LDA, either at –78 or 0 °C gave a complex mixture of products, as did LiTMP at 0 °C. *t*-BuLi gave a mixture of carbonyl addition/substitution products predominating, while *sec*-BuLi gave a complex mixture of products. *n*-BuLi/TMEDA gave predominantly the corresponding *bis*-tertiary alcohol and none of the desired iodide. In the absence of the additive TMEDA, 13a was the major product,

Scheme 1. (a) Established Synthesis of 2,7-Di-*tert*-butyl-*trans*-10b,10c-dimethyldihydropyrene (5) and (b) Proposed Route to 2,7-Diethynyldihydropyrene

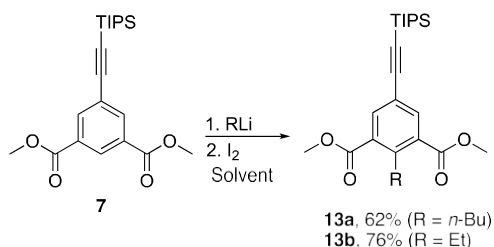
a – Previous work: Established DHP synthesis and late stage functionalization



b – Proposed DHP synthesis with early stage functionalization



Scheme 2. Reaction of Dimethyl Isophthalate 7 with Organolithium Compounds Followed by the Addition of Iodine



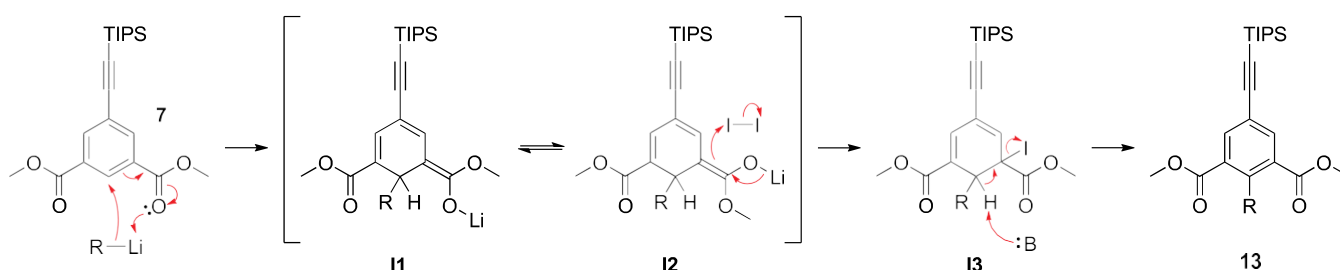
independent of the reaction temperature. Under the same conditions (low temperature, short reaction time) with EtLi, only traces of the ring-ethylated product 13b were formed, but on switching to ether at room temperature, 13b was the major product. MeLi was more reactive (than EtLi) at a low temperature in THF, giving mainly the tertiary alcohols and only a trace of the ring-methylated product. The results suggest that the outcome of the reaction is strongly influenced by the state of aggregation of the organolithium reagent.

Mechanism. Intrigued by the successful ring alkylation of 7, we investigated the mechanism of the reaction. One hypothesis was that metalation was followed by the reaction with *in situ* generated iodoalkane by lithium–halogen exchange. However, additions of tri-*n*-butyltin chloride or excess dry ice after treatment with organolithium gave no arylstannane or carboxylic acid, respectively. A persistent, intensely pink-colored intermediate was observed after addition of the alkyl lithium reagent to 7, which is suggestive of Meisenheimer-like intermediates. Attempts were made to characterize these intermediates by NMR spectroscopy. ¹H and ¹³C NMR spectra suggest the presence of a complex mixture of, possibly, geometric isomers.

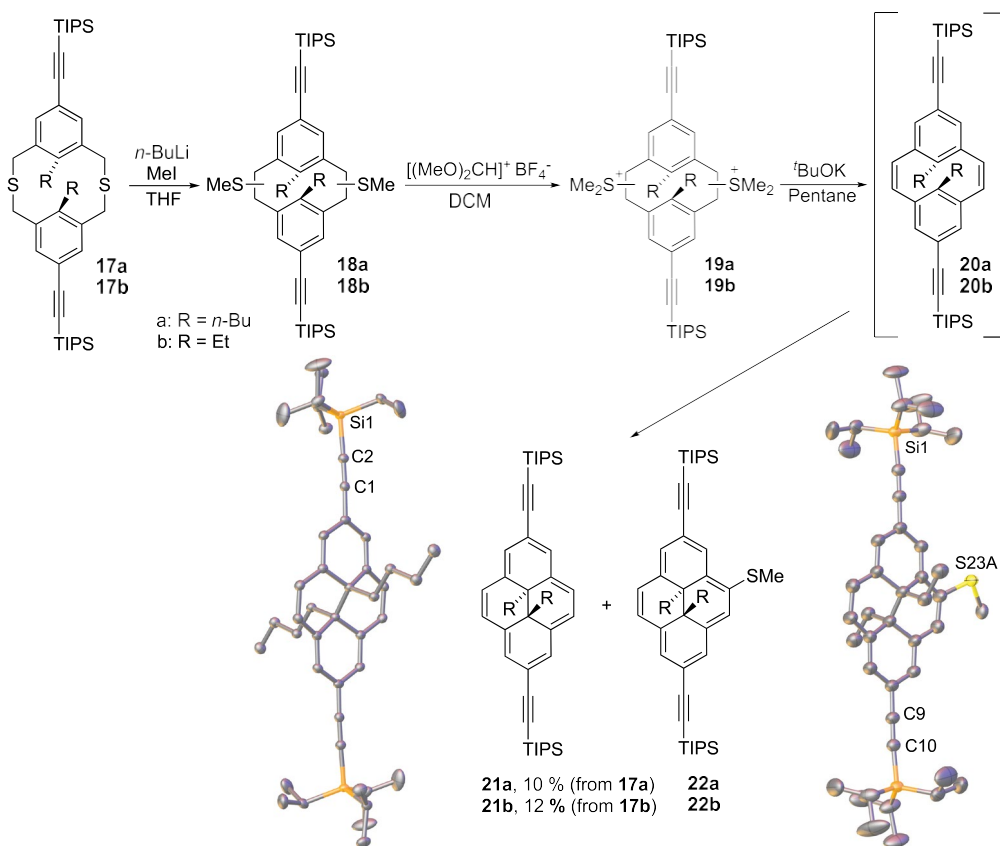
Based on the products obtained and observations described above, the mechanism shown in Scheme 3 is proposed. Nucleophilic addition of alkyl lithium to the most electrophilic ring carbon in 7 results in a mixture of Meisenheimer-like stabilized lithium enolate intermediates I1 and I2, which are responsible for the intensely pink color. In addition to E/Z isomerism, variable aggregation possibly contributes to the complex NMR spectra observed for these intermediates.

Iodination of enolates I1/I2 to give I3, followed by elimination of HI results in net oxidative rearomatization.

Scheme 3. Proposed Mechanism of Nucleophilic Oxidative Alkylation of 7



Scheme 4. Synthesis of 2,7-Diethynyl-DHPs, Starting from Metacyclophanes 17a/b and Representations of Molecular Structures of DHPs 21a and Thiomethyl-DHP 22b as Determined by X-ray Crystallography^a



^aHydrogen atoms are omitted for clarity. Atomic displacement ellipsoids are shown at a probability level of 50% for 21a and 30% for 22b.

Indeed, small quantities of 13b were observed to form upon long-term storage of the intermediates (putatively 11/12 with R = Et) under Ar, presumably triggered by trace oxygen entering the vessel. While oxidative alkylation of electron-deficient heterocycles with alkyllithium reagents, such as *n*-BuLi⁴⁹ and MgEt₂-EtLi mixtures,⁵⁰ is reasonably well known, reports of such transition-metal-free transformations on substituted benzenes are restricted to nitrobenzenes,^{48,51–57} often with DDQ used as the oxidant. To the best of our knowledge, the reaction is unprecedented for benzoates. Interestingly, when the reaction of organolithium reagents with dimethyl isophthalate was attempted, only carbonyl addition (substitution) products were observed, suggesting that the ethynyl substituent stabilized the putative Meisenheimer complex.

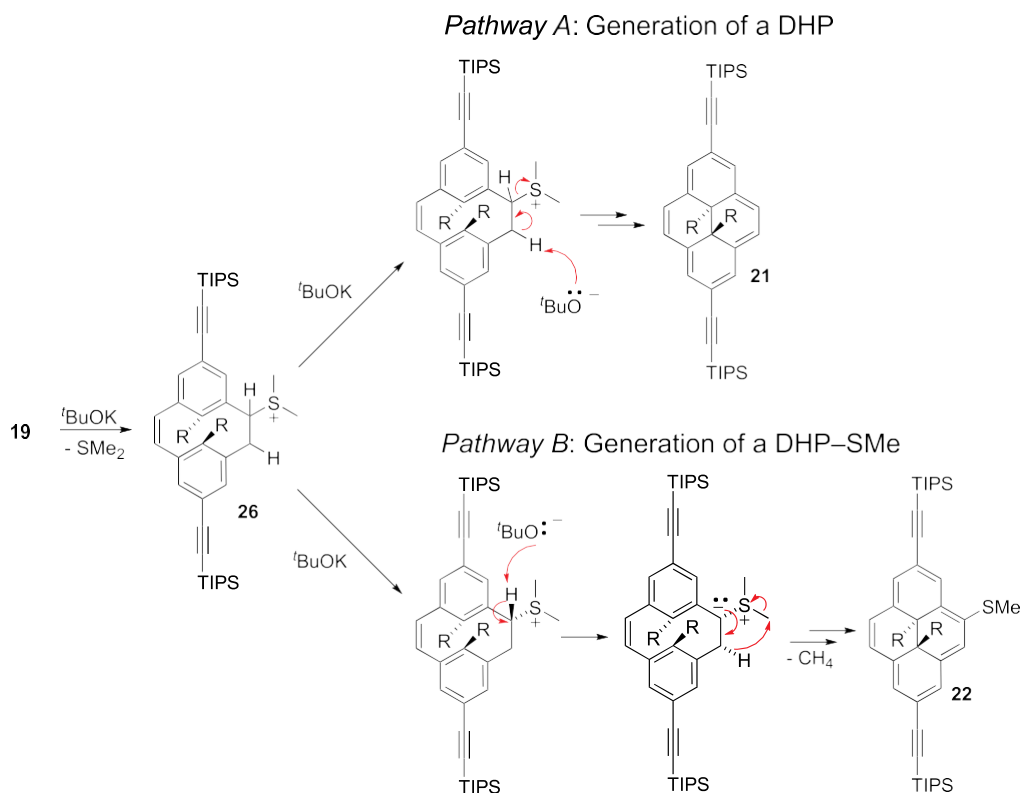
Having 13a and 13b in hand, the preparation of DHPs was pursued (Schemes 4 and S1). Reduction to alcohols 14a/b and subsequent conversion to dibromides 15a/b proceeded in good yield (see Scheme S1 for structures of the intermediates). All of them were characterized by X-ray crystallography (Figure S2). While most macrocyclizations to give *bis*-thioether metacyclophanes have been carried out with dithiols, we chose *bis*-thioacetates.⁵⁸ This reduces the number of steps by one, and thioacetates are air-stable, whereas the dithiols are prone to oxidative disulfide formation. The reaction of bromides 15a/b with thioacetates 16a/b under high dilution conditions generated symmetrical metacyclophanes 17a and 17b in good yield (Scheme S1). Isolation of pure *anti*-metacyclophanes 17a/b was achieved by recrystallization.

Their molecular structures, as determined by X-ray diffraction, are depicted in Figure S2.

Metacyclophanes 17a/b were converted to corresponding DHPs via established routes,^{31,59} beginning with a 1,2-Wittig rearrangement induced by treatment with *n*-BuLi, followed by *in situ* trapping of intermediate dithiolates with methyl iodide. This gave mixtures of isomeric ring-contracted thioethers 18a/b (Scheme 4). As expected, NMR spectra of these mixtures are complex, but their APCI mass spectra were comparatively simple and elemental analyses gave satisfactory results. Further methylation with dimethoxycarbonium tetrafluoroborate (Borch reagent) presumably gave the corresponding sulfonium salts 19a/b. The crude intermediates were subjected to a Hofmann-like elimination by treatment with *t*-BuOK in THF.

While the route outlined in Scheme 4 works well for many DHPs, it afforded target compounds 21a/b only in trace amounts. Using this methodology, low yields have been reported for a chromium–DHP complex,⁶⁰ a DHP with internal naphthalene substituents,⁶¹ and an unsubstituted DHP bearing internal alkyne groups.³¹ In the current work, an important early observation was that standard elimination conditions produced unusual DHP side-products in a similarly low yield. The purple-colored DHPs, which were slightly more polar than the desired targets, bear a thiomethyl group in the 5-position (22a/b, Scheme 5). This substituent results in desymmetrization and the generation of two stereocenters, as reflected in the increase in complexity of the internal alkyl group signals in the ¹H NMR spectra of 22a/b, relative to 21a/b. The chemical shift range of the internal alkyl

Scheme 5. Generation of the Desired DHPs (Pathway A) and a Competing Side-Reaction Leading to the Formation of 4-Thiomethyl-DHP (Pathway B)



substituents in the ^1H NMR spectrum of the crude mixture from preparation 21b is shown in Figure S1.

A comparable side-product was observed during the final Hofmann-like elimination leading to the synthesis of an aza-DHP containing a bridgehead nitrogen atom⁶² and for a pyrene derivative;⁶³ in the latter case, a 1,4-sigmatropic rearrangement with elimination of methane was proposed to explain its formation. A possible mechanism for the formation of thiomethyl derivatives 22 is set out in Scheme 5, in a similar fashion as described for naphthalene-based paracyclophanes.^{64,65}

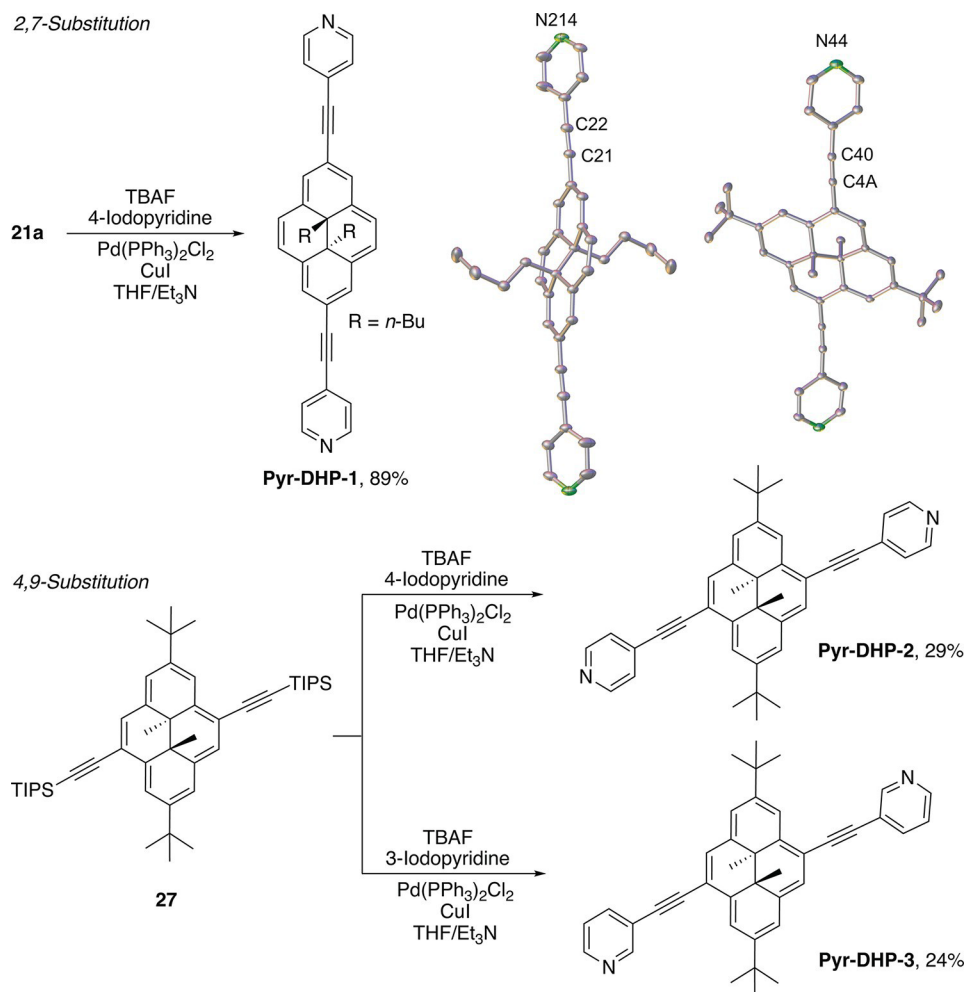
The desired pathway (A) involves successive Hofmann-like (β) elimination reactions of each dimethyl sulfide leaving group in 19, via 26 and to give cyclophane 20, which then undergoes isomerization to DHP 21. However, deprotonation can also occur in α -position to a sulfonium group in 19 or 26 resulting in ylide formation, as illustrated for 26, in the alternative pathway (B). The resulting 27 can undergo [1,4]-sigmatropic rearrangement with the loss of methane, leading to the observed thiomethyl DHP 22. α -Deprotonation can also occur at both positions, which in turn results in the formation of various other possible isomers. We characterized several of these fragments from the preparation of DHP 21a by mass spectrometry by fractions obtained from preparative thin layer chromatography. These side-reactions are the main reason behind the low yields of DHPs reported here.

We attempted to improve the final Hofmann-like elimination step by suppressing the described side-reactions. Methylations of 18 with Borch reagent in DCM to give sulfonium salts 19 are followed by solvent removal and purification of the solids remaining by washing with EtOAc,

which deactivates and removes the excess Borch reagent. This works well for the preparation of many DHPs but fails in the current case as 19a/b are both too soluble in EtOAc and no separation is achieved. For the subsequent deprotonation in THF, 3 equiv of *t*-BuOK were found to be optimal, with less failing to generate DHP and more leading to decomposition. As such, increasing the amount of *t*-BuOK to deactivate the excess Borch reagent in THF was not a viable option. However, this step has been exclusively reported in THF (representative examples^{31,60,66}). We were initially able to isolate small amounts of DHPs prepared under the standard conditions in THF albeit accompanied by thiomethyl DHPs 22. The elimination step was repeated in toluene, diethyl ether, or pentane and proceeded in all solvents. In toluene and diethyl ether, DHPs 21 were formed at room temperature, but the thiomethyl side-products 22 were produced in similar quantities. Pentane gave the best results as less side-products formed. The sulfonium salts 19 and *t*-BuOK are poorly soluble in pentane, and thus the reaction proceeds significantly slower than in other solvents, and it could be this fact that suppresses the formation of 22. A larger excess of *t*-BuOK (7.5 equiv) could be used in pentane avoiding the need to triturate crude sulfonium salts with EtOAc. This modification led to a further improvement in yield, affording the target DHPs in workable yields of 10–12% over the last three steps. The low yields likely originate in a complex combination of several factors, which includes the unexpected side-reaction likely facilitated by the presence of the TIPS-alkyne substituents.

Molecular structures of 21a, 21b, and 22b were obtained from X-ray single-crystal diffraction experiments. The structures of 21a and 22b are depicted in Scheme 4. We have reported the X-ray structure of 22b, and its unusual

Scheme 6. Syntheses of the Target DHPs for Single-Molecule Conductance Studies^a



^a(a) Derivatives with surface-anchoring groups in 2,7-positions. (b) Derivatives with surface-anchoring groups in 4,9-positions; and representations of the molecular structures of Pyr-DHP-1 and Pyr-DHP-2 as determined by X-ray crystallography. Hydrogen atoms are omitted for clarity. Atomic displacement ellipsoids are shown at a probability level of 30% for Pyr-DHP-1 and 50% for Pyr-DHP-2.

thermal single-crystal-to-single-crystal transformation elsewhere.⁶⁷

Syntheses of Target Molecules for Conductance Studies. Having established a viable route to the TIPS-protected DHPs 21, we proceeded with installing 4-pyridyl substituents as electrode-anchoring groups by *in situ* deprotection and Sonogashira coupling with 4-iodopyridine, yielding Pyr-DHP-1 from 21a (Scheme 6). Pyridine moieties were chosen for anchoring to the gold electrodes as they have been shown to be effective in forming robust single-molecule junctions.⁶⁸ Pyridyl anchoring groups bind to gold through the N-lone pair on their terminal nitrogen. Although the Au–N binding energy is considerably weaker than Au-thiolate contacting, it is noteworthy that strongly chemisorbed electrode contact groups have shown to be detrimental to photochemical processes without appropriate decoupling spacer groups, as evident in diarylethene single-molecule junctions.²⁰ Alkynyl spacer groups were selected to allow increased conjugation across the single-molecule junction and thereby increase the single-molecule conductance.

For comparison, we synthesized two DHPs with pyridyl anchor groups, tethered by alkynyl linkers to the 4,9-positions. For this, the well-known 4,9-dibromo DHP (26, Scheme S2)

was subjected to Sonogashira coupling reaction to afford DHP 27 (Schemes 1 and S2). Deprotection yielded bis alkyne 28, which was used for coupling with 4-iodopyridine and 3-iodopyridine to give Pyr-DHP-2 and Pyr-DHP-3, respectively. The molecular structures of Pyr-DHP-1 and Pyr-DHP-2 are shown in Scheme 6.

Structurally comparable, although flat, alkylated and non-alkylated pyrene derivatives bearing two pyridyl substituents were synthesized recently by similar C–C coupling reactions from brominated pyrenes and Bpin-pyridines.⁶⁹

Molecular Properties of DHPs. Switching. We attempted to photochemically switch Pyr-DHP-1, Pyr-DHP-2, Pyr-DHP-3, 21a, and 27 to the corresponding CPD isomers using different experimental conditions. Varied parameters included light sources, wavelengths, and solvents (see Supporting Information for details, pp S29–S34). While none of the alkynyl derivatives isomerized fully reversibly to CPD isomers in the experiments, the known DHP 2,7-di-*tert*-butyl-*trans*-10b,10c-dimethyl-10b,10c-dihydropyrene (5, Scheme 1) did isomerize in our experiments. In some instances, when irradiating DHP samples in solution, a decrease or vanishing of characteristic DHP bands was observed in the UV/vis spectrum. During subsequent heating

of the samples, several DHP bands reappeared although at lower intensity. This is ascribed to a significant degree of radical or oxidative decomposition that has been detailed in the literature.^{70,71} Furthermore, many DHPs do not open upon visible light irradiation and a paradigm correlating substituents and excitation wavelength does not exist.³¹

Electrochemistry. We investigated the electrochemical behavior of DHPs by cyclic voltammetry. TIPS-protected compounds 21a, 21b, and 27 were used as model systems, which do not feature surface-contacting groups that could possibly interfere with the electrode surface during the measurement. Cyclic voltammograms (CVs), recorded at a scan rate of 50 mV/s, of all samples exhibit similar features (Figure 2). Cyclic voltammograms recorded at varying scan

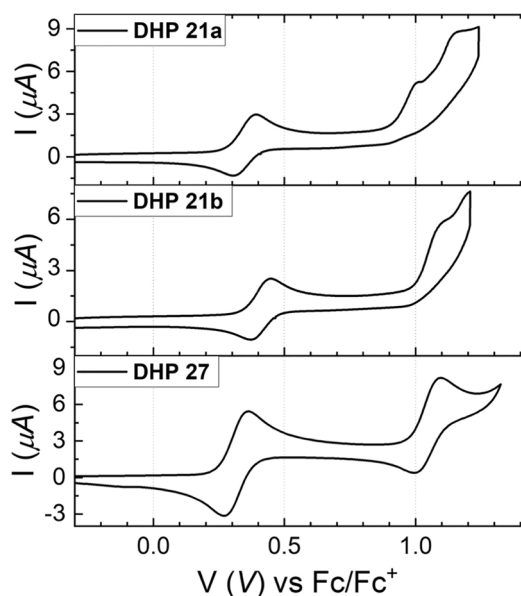


Figure 2. Cyclic voltammograms of DHPs 21a, 21b, and 27 recorded at a scan rate of 50 mV/s with an analyte concentration of 1 mM. The supporting electrolyte was 0.1 M tetrabutylammonium hexafluorophosphate in dichloromethane. All data are reported vs the Fc/Fc⁺ couple.

rates are reported in the Supporting Information (pp S35–S36). Important data are summarized in Table 1. A reversible

Table 1. Summary of Oxidation Potentials Obtained from Cyclic Voltammetry^a

compound	$E_{1/2}$ (DHP/DHP ⁺) [mV]	Ox (DHP ²⁺ /DHP ⁺) [mV]
21a	349	1012/1154 ^b
21b	360	1097 ^b
27	315	1050

^aAll potentials are reported vs the Fc/Fc⁺ couple. ^bThese processes are not well resolved, and the reported values correspond to the peak potentials of the observed oxidation waves (E_{pa}).

redox process attributed to the DHP/DHP⁺ couple is situated at ~+300 mV (vs Fc/Fc⁺), which is in good agreement with other DHPs.²³ Compounds 21a and 21b show essentially the same redox behavior as observed previously with the DHP/DHP⁺ process occurring for 21a slightly below that of 21b (349 mV vs 360 mV), indicative of a subtle increase in the electron-donating ability of the internal butyl group compared to the ethyl group on the DHP system. A slight increase in the

oxidation potential of the first process compared to DHP 5 ($E_{1/2} = 125$ mV (vs Fc/Fc⁺)) is attributed to HOMO stabilization from the alkyne functional groups.⁷² Compound 27, bearing two electron-rich *tert*-butyl groups, shows a lower first oxidation potential of 315 mV.

Oxidation to DHP²⁺ occurs irreversibly for 21a and 21b at +1.0 V and above. In that potential region, the CV of 21a shows two weakly pronounced oxidation peaks, while the CV of 21b shows only one weakly pronounced peak. CVs show an indistinct oxidation peak with no visible return cathodic peak. DHP 27 shows a similar first reversible oxidation; however, it did display a more pronounced return cathodic peak after the second oxidation.

Spectroelectrochemistry. Spectroelectrochemistry is a valuable tool to gain spectroscopic information about electrochemically generated redox species.^{73,74} There are a range of spectroscopic methods that have been coupled to electrochemical scans; here, we conducted spectroelectrochemical measurements on two of the compounds, by electrochemically oxidizing the compounds and recording *in situ* UV/vis spectra. Figure 3 shows the electrode potential-dependent UV/vis spectra, up to a potential inducing the second oxidation (DHP²⁺). First, we have assigned bands in the spectrum recorded at 0.0 V, which corresponds unambiguously to the DHP form, based on both comparison to previous studies of similar compounds^{22,72} and on density functional theory (DFT) calculations (Supporting Information, pp S39–S40).

The initial UV-vis spectrum shows the typical broad absorptions at ca. 350, 420, and 550 nm associated with $\pi-\pi^*$ (¹B and ¹L) transitions of DHP. The additional fine bands are tentatively assigned to $\pi-\pi^*$ transitions from the ethynyl pyridyl functional groups. The large band below 300 nm is assigned to either a charge transfer process or $\pi-\pi^*$ transitions from a lower energy molecular orbital. During the experiment, the potential was ramped up in 0.1 V increments. Up to +0.6 V, no significant changes were observed. At +0.7 V, the intensities of the major DHP-assigned bands begin to decrease, and at +0.8 V a further stark depletion of the bands takes place. At +0.9 V, the intensity decreased slightly further. From this point onward, the spectrum stabilizes, and no significant changes were observed with further increase in the potential. In conjunction with the diminution of DHP-related absorptions, bands at ~300 and 630 nm appear, which we assign to the dication of the open CPD form. Interestingly, when decreasing the applied potential again to 0 V in 0.1 V increments, again at the +0.7 V/+0.6 V step, the newly formed bands start disappearing and simultaneously, DHP-associated bands reappear (Figure 3b). When ramping further down to 0 V, the DHP-assigned bands slowly gain more intensity over each step; but do not reach full intensity immediately. After standing for 45 min, the band intensity again increased substantially.

While oxidations of DHP molecules are associated with significant changes in their UV-vis spectrum,²² the complete disappearance of the ¹B and ¹L bands is typical of DHP-to-CPD isomerization.^{75,76} Coupled with the thermal delay of the return of the original spectrum upon reducing the dication species back to the neutral species, the experiment suggests that the second oxidation of 21b coincides with electrochemical isomerization of DHP to CPD. To further support the hypothesis of electrochemical switching, we calculated the electronic spectra of the DHP and CPD forms and their cations (Figure S15). The simulated spectra match the

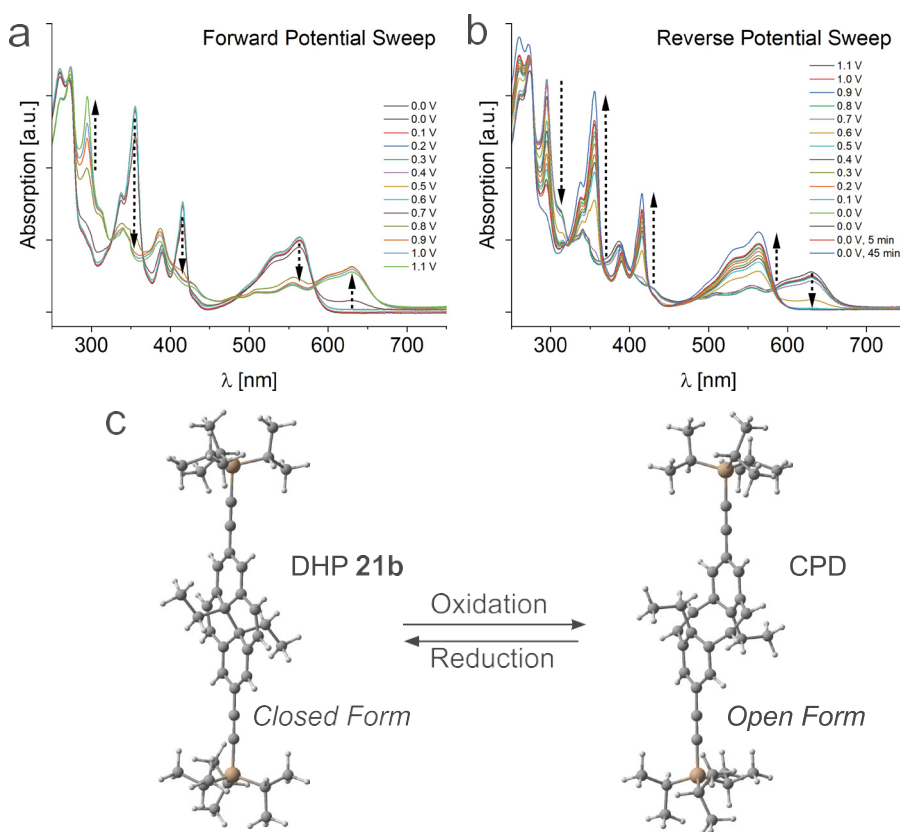


Figure 3. Applied electrochemical potential-dependent UV/vis spectra for DHP 21b: (a) increasing of the potential incremental in 0.1 V steps from 0 to 1.1 V; (b) decreasing of the potential in 0.1 V steps, from 1.1 V back to 0 V. The plot shows two further UV/vis spectra recorded at 5 and 45 min after 0 V was reached. (c) DFT-calculated structures at 6-31G(d) level of theory for the closed DHP form of 21b and the corresponding open cyclophanediene (CPD) form in the dication state.

experiments, i.e., the simulated spectrum of the (closed) DHP matches the spectrum before oxidation and the simulated spectrum of the dication of the (open) CPD isomer matches the one obtained above +0.7 V.

Based on these results, we suggest that 21b electrochemically switches from the DHP to the CPD form upon oxidation to the dication and converts back to DHP upon the decrease of the potential. However, 21b on the reverse scan does not revert to DHP on returning to the starting potential, and full isomerization requires a further 45 min.

We similarly studied DHP 27 by spectroelectrochemistry, as shown in Figure S11. Upon oxidation to the dication, in analogy to compound 21b, the UV/vis spectrum changes substantially with the disappearance of the main bands associated with the typical $\pi-\pi^*$ absorptions of the closed DHP. Upon returning to the starting potential, no immediate spectral changes are observed; however, a gradual return of the spectrum is observed over a 30 min window. This DHP isomerizes at a similar applied potential (~ 0.8 V), but switches back substantially slower as no immediate reversion to DHP is observed upon reduction of the dication species. Again, we have simulated the UV/vis spectra of the neutral open and closed forms of 27 (Figure S16), and the outcome of the simulations matches the experiment for the open and closed form. The slower back thermal reversion at room temperature indicates a higher stability of the open form of this DHP compared to 2,7-ethynyl-substituted derivatives, which is also in line with the successful photochemical switching of a recent

example of similar structure, which is an isomer of Pyr-DHP-2.⁴⁰

Electrochemically assisted isomerization of DHP/CPD systems has been reported for a η^6 -Ru^{II}Cp-benzo-fused CPD that underwent ring-closure upon electrochemical reduction,⁴⁰ for a bis(ferrocenyl)dimethyl DHP,²³ a benzodimethyl DHP,⁷⁷ and other nonbenzo-fused DHPs.^{28,78} While the examples presented here in the spectroelectrochemical experiments are not of exactly the same structure (TIPS vs pyridyl substituents) as the compounds used in the single-molecule junctions below, they may serve as model systems for the latter.

To support our SEC observations of ring opening of the DHP to the CPD form, we undertook the chemical oxidation of samples of 21a/b. The strong oxidant SbCl₅ is capable of receiving more than one electron and is often used when multielectron oxidations are required.⁷⁹ Solutions of 21a and 21b were reacted with 1 and 10 equiv of SbCl₅, respectively, and the resulting mixtures were analyzed spectroscopically (see Supporting Information, p S39). Similar UV-vis spectra of both solutions show the disappearance of bands in the visible region of the electromagnetic spectrum and the growth of bands in the UV region of the spectrum on oxidation. These latter observations are broadly consistent with the calculated spectra of the oxidized products (Figure S15). In the case of DHP 21a, the solution was dried and subsequent ¹H NMR spectrum of the resulting solid confirmed the absence of upfield signals usually attributable to internal alkyl groups of DHP compounds. These data further support our assertion that CPD²⁺ is produced on the 2-electron oxidation of DHP.

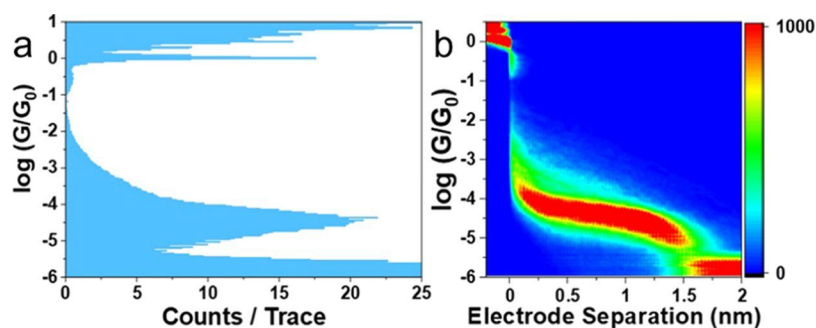
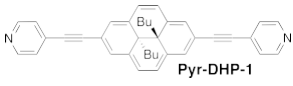
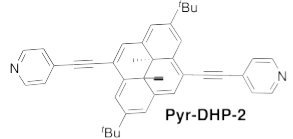
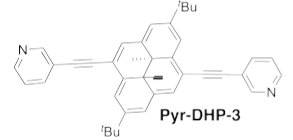
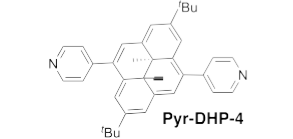


Figure 4. (a) 1D conductance histogram and (b) 2D conductance-electrode displacement map for Pyr-DHP-2 at 100 mV bias. More than 2000 individual breaking traces were compiled with no data selection.

Table 2. Summary of the Conductance and Thermopower Data for the DHPs Studied^a

Dihydropyrene	Conductance [G_0]	Break-Off Distance (95% C.I) [nm]	Seebeck Coefficient S [$\mu\text{V}/\text{K}$]
 Pyr-DHP-1	$10^{-4.15 \pm 0.27}$	1.90	-1.8
 Pyr-DHP-2	$10^{-4.36 \pm 0.31}$	1.60	-3.7
 Pyr-DHP-3	$10^{-4.87 \pm 0.31}$	1.02	3.2
 Pyr-DHP-4	$10^{-4.60 \pm 0.57}$	0.53	n.d.

^aAll conductance values are recorded at 100 mV bias. Break-off distances are at the 95% C.I. and are unadjusted for snap-back. For Pyr-DHP-1 (>2500), Pyr-DHP-2 (>2000), Pyr-DHP-3 (>2500), and Pyr-DHP-4 (>3500), individual breaking traces, parentheses, were compiled with no data selection. n.d. = not determined.

Charge Transport through DHPs in Single-Molecule Junctions. Scanning tunneling microscopy break junctions (STM-BJ)⁸⁰ were used to collect single-molecule conductance data of Pyr-DHP-1, -2, and -3. Particularly relevant to our studies is the report of the charge-transport characteristics of 2,7-di-*tert*-butyl-4,9-dipyridyl-*trans*-10b,10c-dimethyl-10b,10c-dihydropyrene (Pyr-DHP-4), which we also have examined using the STM-BJ method complementing the reported mechanical break junction study (MCBJ).²⁵

In the STM-BJ, an STM is used to drive an Au tip into an Au substrate to form a metallic contact, and the tip is then withdrawn at a constant speed (20 nm/s). During the withdrawal process, the nanocontact thins to an atomic point contact, having conductance quantum equal to G_0 ($2e^2/h = 77.48 \mu\text{S}$). Further withdrawal breaks the point contact and generates a nanogap of size ~ 0.5 nm. Molecules with appropriate termini (present as a 1 mM solution in mesitylene) can self-assemble in the gap, thus fabricating the single-molecule junction. The withdrawal process is continued to

stretch the molecule to its fully extended state and to then rupture the junction. The tip is driven again into the substrate and the process repeated thousands of times to acquire statistically significant data, which is compiled in statistical histograms and 2D density maps, where features at conductance values $\ll G_0$ are attributed to transport through the molecular wire.

Figure 4 shows the single-molecule conductance of Pyr-DHP-2 at 100 mV bias as an example. Pyr-DHP-2 shows a conductance feature centered at *ca.* $10^{-4.4} G_0$ with an unadjusted plateau length of 1.60 nm (2.20 nm after snap-back adjustment). Pyr-DHP-2 shows the formation of extended plateaus in the 2D histogram and a clear and sharp 1D histogram peak consistent with the N–N separation (1.87 nm) calculated from the crystal structure (see Figure 1c).

Irradiation of the break junction cell containing the Pyr-DHP-2 solution with visible light resulted in no change in the observed junction conductance. Since Pyr-DHP-2 has the DHP core connected directly to alkyne groups, it is important

to consider how these alkyne spacers might impact the photoswitching of the DHP core. Functionalization of the DHP core with alkyne groups is known to lower ring-opening quantum yields compared to similar derivatives without alkynes, while [e]-annulated DHPs bearing alkynes improved the quantum yields.^{33,75,76,81,82} Nevertheless, an isomer of Pyr-DHP-2, bearing two 2-pyridyl groups instead of the two 4-pyridyl groups used as surface-anchoring groups here, has been switched successfully in solution.⁸³ Our observation of no conductance change in the STM-BJ determination of Pyr-DHP-2 after visible light irradiation implies that the alkyne spacer between the DHP and 4-pyridyl contact group negatively affects the photoswitching behavior. However, we document below positive impacts on the junction formation probability and stability from introducing an alkyne spacer between the DHP and the pyridine contact group. These impacts are evinced by the conductance data measured for 28, resulting from deprotected 27 (Figure S17), and the comparison of that data to that of Pyr-DHP-4 and Pyr-DHP-2.

Table 2 shows the conductance data acquired for Pyr-DHP-1, -2, -3, and -4. Pyr-DHP-1 shows the highest single-molecule conductance of the studied molecules. Additionally, Pyr-DHP-2 shows a slightly higher conductance than Pyr-DHP-4, indicating the positive impact the alkynyl spacers have on this property.

A recent theoretical study predicted a higher conductance ratio for the 2,7-substituted DHP core than that of the 4,9-substituted DHP core as determined by the role of the phase and amplitude of the frontier molecular orbitals.⁸⁴

On the other hand, Pyr-DHP-3 shows a marked decrease in single-molecule conductance and junction length relative to Pyr-DHP-2, as expected due to destructive quantum interference effects of *meta*-substituted contact groups.^{85–87} The slight decrease in nitrogen-to-nitrogen distance does not fully account for the shorter junction length, indicating that other factors play a role such as a reduced averaged junction stretching length for the *meta* connected molecule (Pyr-DHP-3) arising from less favorable junction configuration than the *para*-connected (Pyr-DHP-2) analogue.

The conductance quanta of Pyr-DHP-1 and -2 were measured at 100, 200, 300, 400, and 500 mV bias. Figure 5 collates these data. The conductance peak is seen to gradually shift to lower conductance values as the bias voltage is increased in 100 mV increments from 100 to 500 mV. Our

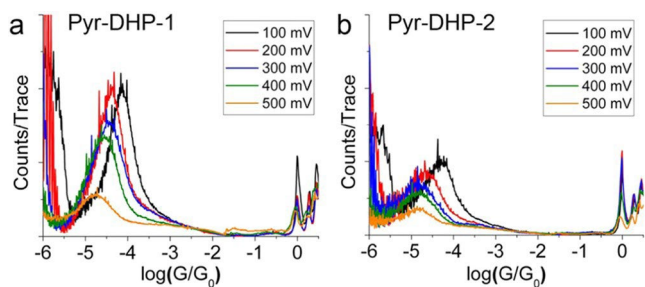


Figure 5. 1D conductance histograms of single-molecule junctions of (a) Pyr-DHP-1 and (b) Pyr-DHP-2 at varying applied bias voltages as marked. For Pyr-DHP-1, more than 2500 individual breaking traces were compiled at each bias with no data selection. For Pyr-DHP-2, more than 2000 individual breaking traces were compiled at each bias with no data selection.

initial hypothesis of this behavior was ascribed to bias-induced isomerization of DHP, although this seemed an unlikely outcome at these relatively low bias-voltage values. Alternatively, the conductance decrease could be attributed to molecular energy levels shifting to off-resonance with increasing bias, although our theoretical computations presented below do not indicate that this might be the case. However, further experiments suggest that junction instability of specific geometries might better explain the observed phenomenon. This argument is discussed further below. A summary of conductance data is collected in Table 2.

To further explore the decreasing conductance with increasing bias voltage described above, current–voltage (I – V) sweeps for Pyr-DHP-2 junctions were recorded. Decreasing conductance (or increasing resistance) with increased bias voltage is referred to as the negative differential resistance (NDR), and it can have various origins.⁸⁸ I – V curves were recorded using a modified STM-BJ method, where a staircase ramp (1 nm step, 100 ms hold) is applied to the STM piezoelectric transducer. During the hold portion, the bias is kept at 100 mV for 25 ms, then swept from -600 to 600 mV at a rate of 24 V/s (50 ms), and finally returned to 100 mV for the remaining 25 ms. Post-collection analysis allowed the selection of events where the junctions were in place. Details on the methods are available elsewhere.⁸⁹ The I – V curves in Figure 6 show no evidence of the decreasing conductance of the junction with increasing bias voltage, in apparent contradiction with the histograms of Figure 5 that clearly show that conductance decreases with increasing bias voltage. However, it should be noted that recording histograms at fixed bias voltage is very different to rapidly measuring I – V curves at fixed junction extension. The fact that these two methods give very different results indicates that the decrease in conductance at higher V_{bias} in the histograms in Figure 5 is a result of junction instability.

To further investigate bias-voltage jumps, Pyr-DHP-2 junctions were created at fixed extension to test their stability and robustness. This technique relies on the same method used for the collection of I – V characteristics, with the voltage jump from 100 to 500 mV and back to 100 mV over 2250 ms intervals. A representative data set is shown in Figure S18. These data also show just a small increase in conductance when the bias voltage is stepped from 100 to 500 mV, while the molecular junction is in place, in good agreement with the I – V characteristic of Pyr-DHP-2. These collective observations suggest that the decreasing conductance with bias voltage is observed only in the 1D histograms and does not have an “electronic” origin due, for example, to reversible charging or chemical change of the molecular bridge. Our calculations also show that the small conformational change that results from the application of an electric field on molecules does not have significant effect on the transmission probabilities. Instead, we suggest that the behavior arises from a bias-voltage-induced instability that only becomes apparent in the histogram data and is not observed in the rapidly measured individual I – V traces. We note that the differences between the data collection of rapid I – V measurements and break junction (histogram) measurements are well known and discussed in the literature and also for the context discussed in the Supporting Information.

Figure 7 shows the 2D histograms for Pyr-DHP-2 at different bias voltages as marked in the figure caption. The 2D histograms show the count density using a color scale at a

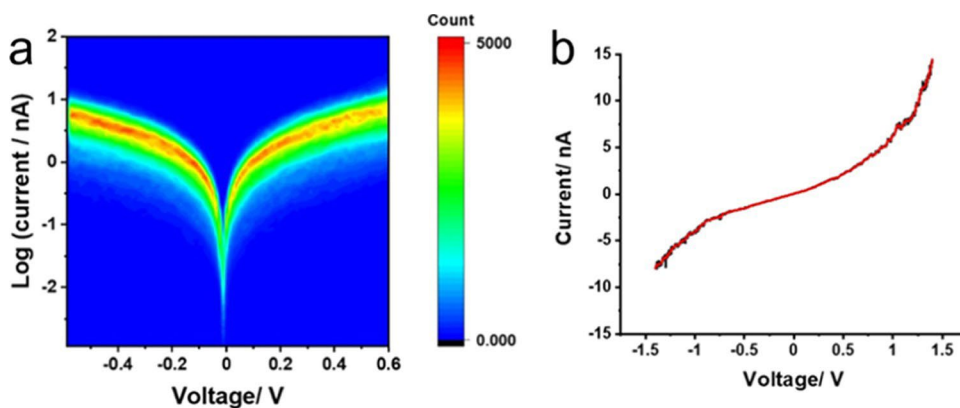


Figure 6. I - V curves recorded for Pyr-DHP-2 single molecular junctions. (a) 2D density map of I - V characteristics for Pyr-DHP-2. (b) Linear average calculated I - V curve (350 scans) for Pyr-DHP-2. A staircase ramp applied to the piezo stretches the junctions in 1 nm intervals for 100 ms. At a hold position, the voltage bias is kept at 100 mV for 25 ms, then swept from -600 to 600 mV at a rate of 24 V/s (50 ms), and finally returned to 100 mV for 25 ms. Plots compiled from 346 out of 1048 raw traces (33% hit rate).

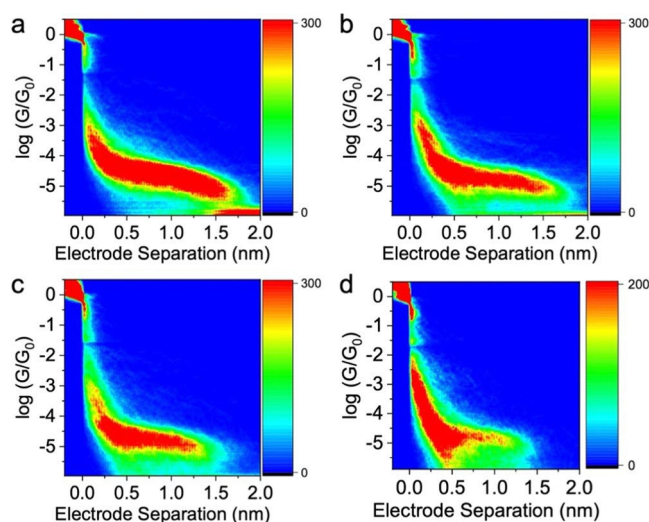


Figure 7. 2D conductance-electrode displacement map for Pyr-DHP-2 at (a) 200 mV, (b) 300 mV, (c) 400 mV, and (d) 500 mV bias. For Pyr-DHP-2, more than 2000 individual breaking traces were compiled at each bias with no data selection.

given conductance (y -axis) vs junction extension (x -axis). These 2D histograms are good for visualizing the junction conductance as it is extended to cleavage. All of these 2D histograms show a long, slightly slanting, conductance plateau in the conductance range between 10^{-4} and $10^{-5} G_0$. At 100 mV bias voltage, a long plateau is observed, which extends to between 1.5 and 2.0 nm (before the addition of the snap-back distance). This long plateau becomes considerably shorter at high bias-voltage values. We attribute this to the junction becoming less stable at high bias-voltage values. Visual analysis of these histograms shows that there is a particular decrease in the propensity of the higher conductance molecular junctions, which is in line with the 1D histograms and shows that the conductance peak shifts in both the height and conductance value as the bias voltage is increased. As molecular conductance peaks would be typically expected to comprise a population from many different junction geometries originating from molecular conformations and contact geometry, we suggest that higher electric fields result in the instability of specific subpopulations of junction geometries leading to a decrease in their formation probability. In

curcuminoid-based molecules, applied bias voltage, using the MCBJ method, was shown to control conformational populations due to interactions of the molecular dipole with the electric field.⁹⁰ Changes in electric fields are known to influence covalent and noncovalent bonds where strong electric fields can even cause bond cleavage.^{91,92} Indeed, the electric field in single-molecule junctions has been used to induce chemical change and promote what has been termed “electrostatic catalysis” in single-molecule electrical junctions.⁹³ Our present results indicate that the electric field also has a dramatic effect on junction stability, conductance, and subpopulation distribution.

The bias-dependent conduction of Pyr-DHP-3 mirrors that of Pyr-DHP-2 for the two biases measured; see Figure S19.

Using a custom-built STM, we are able to simultaneously measure the thermopower and conductance in single-molecule junctions by creating a temperature difference between the tip and the sample.⁹⁴ These measurements help to determine whether the charge transport proceeds through the frontier molecular orbitals of either HOMO or LUMO character.^{94–96} Seebeck coefficients (S , $\mu\text{K}/\text{K}$) for Pyr-DHP-2 and Pyr-DHP-1 were measured as -3.7 and -1.8 $\mu\text{K}/\text{K}$, respectively. The negative sign of the coefficient suggests LUMO conducting systems. Still, the low value indicates that the alignment of the Fermi level (E_F) with respect to the gold electrodes is located more toward the center of the HOMO–LUMO gap rather than as a close alignment between the LUMO and E_F . This phenomenon is typical of pyridine surface-contacting groups. Moreover, the low magnitude of the coefficient suggests that DHP would exhibit poor thermopower performance.

The previously reported Pyr-DHP-4, which was studied using mechanically controlled break junctions (MCBJ),²⁵ was also studied using our STM-BJ. The single-molecule conductance of this compound was measured as a control compound using the STM-BJ and this was then compared to the conductance measured previously in a MCBJ. Figure 8a–c shows 1D and 2D conductance histograms and maps to compare the junction behavior under different bias voltages for Pyr-DHP-4. The conductance of Pyr-DHP-4 from our STM-BJ data is $10^{-46} G_0$, with an unadjusted breaking length of 0.53 nm. This breaking length translates to 1.1 nm when a snap-back correction of 0.6 nm (± 0.25 nm) is added.^{97,98} In previous MCBJ studies of Pyr-DHP-4, three conductance peaks were observed and were correlated to different binding

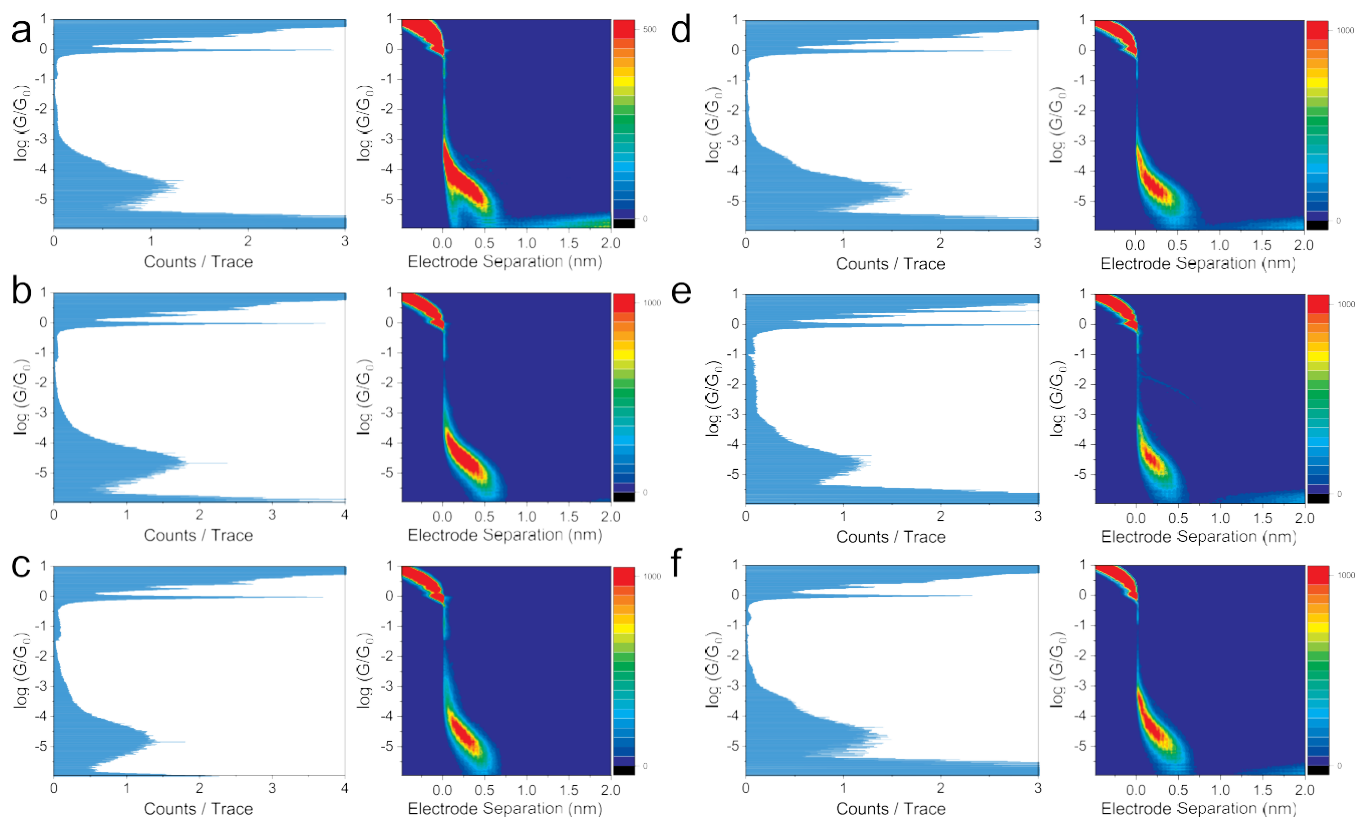


Figure 8. Conductance histograms and conductance–displacement density maps for Pyr-DHP-4 for different bias voltages of (a) 100 mV; (b) 200 mV; (c) 300 mV, and from an irradiation experiment at a bias voltage of 100 mV; (d) prelight exposure, 0.62 JFPR ratio (see main text); (e) after 30 min light exposure, there is a clear decrease in JFPR to 0.38; and (f) after 30 min UV light exposure, 0.63 JFPR ratio. For Pyr-DHP-4, more than 3500 individual breaking traces were compiled at each bias and after irradiation with visible or UV light with no data selection.

configurations. This conductance peak for Pyr-DHP-4 agrees with the median conductance feature in the previously reported MCBJ experiments.²⁵ A slight decrease in junction break-off length is observed as the bias voltage increases, mirroring the phenomenon seen in Pyr-DHP-2.

Apart from the agreement between conductance values seen here for Pyr-DHP-4 with the STM-BJ and the median conductance value determined using the MCBJ, there are some notable differences. Rather than the multiple conductance features seen by Roldan et al.,²⁵ a single well-defined conductance peak is observed. This observation implies that the junction formation and breaking depends on the precise conditions and differs between the STM-BJ experiments here and previous MCBJ ones.²⁵

Figure 8d–f shows histogram and conductance–distance profiles with a 100 mV bias voltage for Pyr-DHP-4 following photochemical irradiation. A solution of Pyr-DHP-4 was irradiated *in situ* in the STM solution cell with visible light through an orange and UV filter, and single molecular conductance was re-collected following this irradiation.

To compare these data in the 1D histograms, we take a ratio between the height of the molecular peak (in counts per trace) and the height of the G_0 trace (also in counts per trace). This is used as an approximate semiquantitative guide to the formation probability of single-molecule junctions. We call this dimensionless value the junction formation probability ratio (JFPR), and smaller values within a given experimental set indicate that molecular junctions are formed with less probability or are less defined. For each of the 1D conductance histograms in Figure 8, the JFPR values are quoted. Before

irradiation, the JFPR is 0.62, which substantially decreases to 0.38 following visible light irradiation. We attribute this decrease in JFPR to the partial conversion of Pyr-DHP-4 to the open CPD (Pyr-CPD-4) form upon visible light irradiation. In agreement with previous results, no extra conductance features are seen for Pyr-CPD-4, which are predicted to fall below the noise floor. However, there are differences to previous MCBJ data, which indicated that 100% photochemical conversion might be possible. Our new results show only partial conversion, which agrees with findings from other measurement techniques. This suggests that either partial photo-conversion is attained or that during the experiment, Pyr-CPD-4 is converting back to Pyr-DHP-4 because of the thermal back-reaction. Of relevance here is a first-principles study by Hu et al. that showed that the thermal activation energy of CPD to DHP isomerization decreases when placed between gold electrodes, when compared to that of the calculated gas phase.²⁴ Following the visible light irradiation and conductance measurements shown in Figure 8, the same (*in situ*) STM sample was irradiated with UV light and conductance data re-recorded. These data give a JFPR of 0.63, showing that this ratio reverts to close to the original value of 0.62. This indicates reversible switching back to the original Pyr-DHP-4 isomer.

Theoretical Calculations. To better understand the charge transport in Pyr-DHPs (1–4), we used density functional theory (DFT)⁹⁹ combined with quantum transport calculations to compute the charge-transport properties of the molecules with different connectivities. The optimized geometry and ground-state Hamiltonian and overlap matrix

elements of each structure studied in this paper were self-consistently obtained using the SIESTA implementation of density functional theory (DFT). SIESTA employs norm-conserving pseudo-potentials to account for the core electrons and linear combinations of atomic orbitals to construct the valence states. A Generalized Gradient Approximation (GGA) functional is used with Perdew–Burke–Ernzerhof (PBE) parameterization. A real-space grid was defined with an equivalent energy cut-off of 250 Ry. From the mean-field Hamiltonian of the converged molecular structures obtained from DFT, we calculate the transmission coefficient $T(E)$ ¹⁰⁰ for electrons of energy E passing from the source to the drain electrode via the molecule using the transport code Gollum^{99,101} (see the Method section in the [Supporting Information](#) for details). We found that the best agreement with the experiment is obtained at $E = -0.5$ eV close to the middle of HOMO–LUMO gap toward LUMO resonance. This is consistent with the thermopower measurement where we found negative Seebeck coefficient that indicates LUMO transport. The conductances at this Fermi energy are $10^{-4.0}$, $10^{-4.45}$, $10^{-8.7}$, and $10^{-4.65}$ for Pyr-DHP(1–4), respectively, as illustrated in [Figure 9](#) and follows the order: Pyr-DHP-1 > Pyr-DHP-2 > Pyr-DHP-4 > Pyr-DHP-3 in agreement with the experiment.

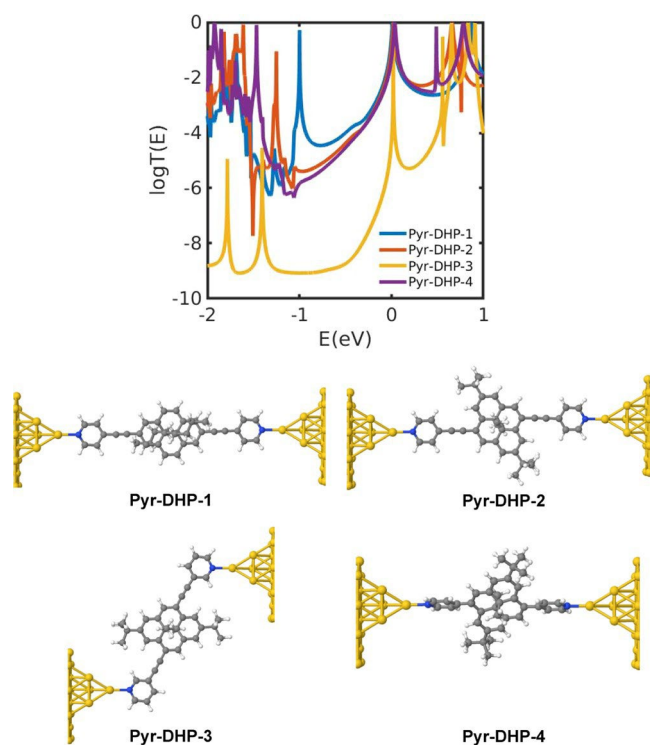


Figure 9. DFT-based transmission coefficients of the compounds Pyr-DHP-1, Pyr-DHP-2, Pyr-DHP-3, and Pyr-DHP-4, and their relaxed structures between gold electrodes.

CONCLUSIONS

We have developed a viable synthetic route to dihydropyrene (DHP) molecular switches bearing surface-contacting groups, connected via alkynes, in the 2,7-carbon atom positions. The multistep route was enabled through a nucleophilic oxidative alkylation of an isophthalate diester precursor, and reactions enroute were studied in detail. Further DHP derivatives with

surface-contacting groups in 4,9-carbon atom positions were prepared by conventional routes. Molecular properties of DHPs were studied by cyclic voltammetry, spectroelectrochemistry, and light irradiation experiments. Spectroelectrochemistry on two representative 2,7- and 4,9- examples showed electrochemical ring opening to the cyclophanediene (CPD) isomers at elevated redox potentials. DHP-CPD isomerization pathways through light, heat, and electrochemical stimulus were investigated by DFT calculations. Single-molecule STM break junctions using Au electrodes were fabricated from derivatives with pyridyl surface-contacting groups. Charge-transport capabilities of the 2,7-substituted derivatives were juxtaposed against the 4,9-substituted analogues and a similar molecule lacking an ethynylene spacer. All DHPs with pyridyl surface-anchoring groups interrogated in this study form stable molecular junctions at 100 mV voltage bias with break-off distances corresponding to experimentally determined molecular lengths; however, at higher biases, we observed a destabilization of junction formation and stability.

AUTHOR INFORMATION

Corresponding Author

George A. Koutsantonis – *Chemistry, School of Molecular Sciences, The University of Western Australia, Crawley, WA 6009, Australia*; orcid.org/0000-0001-8755-3596; Email: george.koutsantonis@uwa.edu.au

Authors

Max Roemer – *Chemistry, School of Molecular Sciences, The University of Western Australia, Crawley, WA 6009, Australia*; Present Address: The University of Sydney, School of Chemistry, Sydney, NSW 2006, Australia; orcid.org/0000-0003-4876-8011

Angus Gillespie – *Chemistry, School of Molecular Sciences, The University of Western Australia, Crawley, WA 6009, Australia*

David Jago – *Chemistry, School of Molecular Sciences, The University of Western Australia, Crawley, WA 6009, Australia*

David Costa-Milan – *Department of Chemistry, University of Liverpool, Liverpool L69 7ZD, United Kingdom*

Jehan Alqahtani – *Department of Physics, King Khalid University, Abha 62529, Saudi Arabia*; *Department of Physics, Lancaster University, Lancaster LA1 4YB, United Kingdom*

Juan Hurtado-Gallego – *Condensed Matter Physics Center (IFIMAC) and Instituto Universitario de Ciencia de Materiales “Nicolás Cabrera” (INC), Universidad Autónoma de Madrid, E-28049 Madrid, Spain*; orcid.org/0000-0001-7036-5687

Hatef Sadeghi – *School of Engineering, University of Warwick, Coventry CV4 7AL, United Kingdom*; orcid.org/0000-0001-5398-8620

Colin J. Lambert – *Department of Physics, Lancaster University, Lancaster LA1 4YB, United Kingdom*; orcid.org/0000-0003-2332-9610

Peter R. Spackman – *Chemistry, School of Molecular Sciences, The University of Western Australia, Crawley, WA 6009, Australia*; Present Address: Curtin Institute for Computation, School of Molecular and Life Sciences, Curtin University, Perth, WA 6845, Australia; orcid.org/0000-0002-6532-8571

Alexandre N. Sobolev – *Centre for Microscopy, Characterisation and Analysis, The University of Western Australia, Crawley, WA 6009, Australia*

Brian W. Skelton – *Chemistry, School of Molecular Sciences, The University of Western Australia, Crawley, WA 6009, Australia*; *Centre for Microscopy, Characterisation and Analysis, The University of Western Australia, Crawley, WA 6009, Australia*

Arnaud Grosjean – *Chemistry, School of Molecular Sciences, The University of Western Australia, Crawley, WA 6009, Australia*

Mark Walkey – *Chemistry, School of Molecular Sciences, The University of Western Australia, Crawley, WA 6009, Australia*

Sven Kampmann – *Chemistry, School of Molecular Sciences, The University of Western Australia, Crawley, WA 6009, Australia*

Andrea Vezzoli – *Department of Chemistry, University of Liverpool, Liverpool L69 7ZD, United Kingdom*; orcid.org/0000-0002-8059-0113

Peter V. Simpson – *School of Molecular and Life Sciences, Curtin University, Perth, WA 6102, Australia*

Massimiliano Massi – *School of Molecular and Life Sciences, Curtin University, Perth, WA 6102, Australia*; orcid.org/0000-0001-6949-4019

Inco Planje – *Department of Chemistry, University of Liverpool, Liverpool L69 7ZD, United Kingdom*; orcid.org/0000-0003-2188-8611

Gabino Rubio-Bollinger – *Condensed Matter Physics Center (IFIMAC) and Instituto Universitario de Ciencia de Materiales “Nicolás Cabrera” (INC), Universidad Autónoma de Madrid, E-28049 Madrid, Spain*; orcid.org/0000-0001-7864-8980

Nicolás Agraït – *Condensed Matter Physics Center (IFIMAC) and Instituto Universitario de Ciencia de Materiales “Nicolás Cabrera” (INC), Universidad Autónoma de Madrid, E-28049 Madrid, Spain*; *Instituto Madrileño de Estudios Avanzados en Nanociencia IMDEA-Nanociencia, E-28049 Madrid, Spain*; orcid.org/0000-0003-4840-5851

Simon J. Higgins – *Department of Chemistry, University of Liverpool, Liverpool L69 7ZD, United Kingdom*

Sara Sangtarash – *School of Engineering, University of Warwick, Coventry CV4 7AL, United Kingdom*

Matthew J. Piggott – *Chemistry, School of Molecular Sciences, The University of Western Australia, Crawley, WA 6009, Australia*; orcid.org/0000-0002-5857-7051

Richard J. Nichols – *Department of Chemistry, University of Liverpool, Liverpool L69 7ZD, United Kingdom*

ACKNOWLEDGEMENTS

This research was supported under the Australian Research Council's Discovery Projects funding scheme (Project Numbers DP 150104117 and DP 200101659). The authors acknowledge the facilities and the scientific and technical assistance of the Australian Microscopy and Microanalysis Research Facility at the Centre for Microscopy, Characterisation, and Analysis, The University of Western Australia, a facility funded by the University, State and Commonwealth Governments. D.C.-M. gratefully acknowledges the School of Physical Sciences Postdoctoral Development Award of the University of Liverpool for financial support. The work in Warwick was funded by UKRI Future Leaders Fellowship Number MR/S015329/2 and Leverhulme Trust Early Career Fellowship Number ECF-2018-375. A.V. thanks the Royal Society for funding (URF\R1\191241). The work in King Khalid University used the resources of the Supercomputing Laboratory at King Abdullah University of Science & Technology (KAUST) in Thuwal, Saudi Arabia.

REFERENCES

- (1) Marqués-González, S.; Low, P. J. Molecular Electronics: History and Fundamentals. *Aust. J. Chem.* 2016, *69*, 244–253.
- (2) Aradhya, S. V.; Venkataraman, L. Single-molecule junctions beyond electronic transport. *Nat. Nanotechnol.* 2013, *8*, 399–410.
- (3) Jia, C.; Guo, X. Molecule–electrode interfaces in molecular electronic devices. *Chem. Soc. Rev.* 2013, *42*, 5642.
- (4) Xiang, D.; Wang, X.; Jia, C.; Lee, T.; Guo, X. Molecular-Scale Electronics: From Concept to Function. *Chem. Rev.* 2016, *116*, 4318–4440.
- (5) Bergren, A. J.; Zeer-Wanklyn, L.; Semple, M.; Pekas, N.; Szeto, B.; McCreery, R. L. Musical molecules: the molecular junction as an active component in audio distortion circuits. *J. Phys.: Condens. Matter* 2016, *28*, No. 094011.
- (6) Low, P. J.; Marques-Gonzalez, S. Molecular Wires: An Overview of the Building Blocks of Molecular Electronics. In *Single-Molecule Electronics: An Introduction to Synthesis, Measurement and Theory*, Springer, 2016; pp 87–116.
- (7) Díez-Pérez, I.; Hihath, J.; Lee, Y.; Yu, L.; Adamska, L.; Kozhushner, M. A.; Oleynik, I. I.; Tao, N. Rectification and stability of a single molecular diode with controlled orientation. *Nat. Chem.* 2009, *1*, 635–641.
- (8) Zhang, J. L.; Zhong, J. Q.; Lin, J. D.; Hu, W. P.; Wu, K.; Xu, G. Q.; Wee, A. T. S.; Chen, W. Towards single molecule switches. *Chem. Soc. Rev.* 2015, *44*, 2998–3022.
- (9) Aviram, A.; Ratner, M. A. Molecular Rectifiers. *Chem. Phys. Lett.* 1974, *29*, 277–283.
- (10) Capozzi, B.; Xia, J.; Adak, O.; Dell, E. J.; Liu, Z. F.; Taylor, J. C.; Neaton, J. B.; Campos, L. M.; Venkataraman, L. Single-molecule diodes with high rectification ratios through environmental control. *Nat. Nanotechnol.* 2015, *10*, 522–527.

- (11) Elbing, M.; Ochs, R.; Koentopp, M.; Fischer, M.; von Hanisch, C.; Weigend, F.; Evers, F.; Weber, H. B.; Mayor, M. A single-molecule diode. *Proc. Natl. Acad. Sci. U.S.A.* 2005, *102*, 8815–8820.
- (12) Chen, X.; Roemer, M.; Yuan, L.; Du, W.; Thompson, D.; del Barco, E.; Nijhuis, C. A. Molecular diodes with rectification ratios exceeding 10^5 driven by electrostatic interactions. *Nat. Nanotechnol.* 2017, *12*, 797–803.
- (13) Han, Y.; Nickle, C.; Zhang, Z.; Astier, H. P. A. G.; Duffin, T. J.; Qi, D.; Wang, Z.; del Barco, E.; Thompson, D.; Nijhuis, C. A. Electric-field-driven Dual-functional Molecular Switches in Tunnel Junctions. *Nat. Mater.* 2020, *19*, 843–848.
- (14) Song, P.; Guerin, S.; Tan, S. J. R.; Annadata, H. V.; Yu, X.; Scully, M.; Han, Y. M.; Roemer, M.; Loh, K. P.; Thompson, D.; Nijhuis, C. A. Stable Molecular Diodes Based on π - π Interactions of the Molecular Frontier Orbitals with Graphene Electrodes. *Adv. Mater.* 2018, *30*, No. 1706322.
- (15) Huang, X.; Li, T. Recent progress in the development of molecular-scale electronics based on photoswitchable molecules. *J. Mater. Chem. C* 2020, *8*, 821–848.
- (16) Lambert, C. J. Basic concepts of quantum interference and electron transport in single-molecule electronics. *Chem. Soc. Rev.* 2015, *44*, 875–888.
- (17) Sun, L.; Diaz-Fernandez, Y. A.; Gschneidner, T. A.; Westerlund, F.; Lara-Avila, S.; Moth-Poulsen, K. Single-molecule electronics: from chemical design to functional devices. *Chem. Soc. Rev.* 2014, *43*, 7378–7411.
- (18) Mishchenko, A.; Vonlanthen, D.; Meded, V.; Bürkle, M.; Li, C.; Pobelov, I. V.; Bagrets, A.; Viljas, J. K.; Pauly, F.; Evers, F.; Mayor, M.; Wandlowski, T. Influence of Conformation on Conductance of Biphenyl-Dithiol Single-Molecule Contacts. *Nano Lett.* 2010, *10*, 156–163.
- (19) Irie, M.; Fukaminato, T.; Matsuda, K.; Kobatake, S. Photochromism of Diarylethene Molecules and Crystals: Memories, Switches, and Actuators. *Chem. Rev.* 2014, *114*, 12174–12277.
- (20) Jia, C.; Migliore, A.; Xin, N.; Huang, S.; Wang, J.; Yang, Q.; Wang, S.; Chen, H.; Wang, D.; Feng, B.; Liu, Z.; Zhang, G.; Qu, D.-H.; Tian, H.; Ratner, M. A.; Xu, H. Q.; Nitzan, A.; Guo, X. Covalently bonded single-molecule junctions with stable and reversible photo-switched conductivity. *Science* 2016, *352*, 1443–1445.
- (21) Hnid, I.; Frath, D.; Lafolet, F.; Sun, X.; Lacroix, J.-C. Highly Efficient Photoswitch in Diarylethene-Based Molecular Junctions. *J. Am. Chem. Soc.* 2020, *142*, 7732–7736.
- (22) Muratsugu, S.; Kishida, M.; Sakamoto, R.; Nishihara, H. Comparative Study of Photochromic Ferrocene-Conjugated Dimethyldihydropyrene Derivatives. *Chem. – Eur. J.* 2013, *19*, 17314–17327.
- (23) Muratsugu, S.; Kume, S.; Nishihara, H. Redox-Assisted Ring Closing Reaction of the Photogenerated Cyclophanediene Form of Bis(ferrocenyl)dimethyldihydropyrene with Interferrocene Electronic Communication Switching. *J. Am. Chem. Soc.* 2008, *130*, 7204–7205.
- (24) Hu, W.; Zhang, G.-P.; Duan, S.; Fu, Q.; Luo, Y. Molecular Design to Enhance the Thermal Stability of a Photo Switchable Molecular Junction Based on Dimethyldihydropyrene and Cyclophanediene Isomerization. *J. Phys. Chem. C* 2015, *119*, 11468–11474.
- (25) Roldan, D.; Kaliginedi, V.; Cobo, S.; Kolivoska, V.; Bucher, C.; Hong, W.; Royal, G.; Wandlowski, T. Charge transport in photoswitchable dimethyldihydropyrene-type single-molecule junctions. *J. Am. Chem. Soc.* 2013, *135*, 5974–5977.
- (26) Andréasson, J.; Straight, S. D.; Bandyopadhyay, S.; Mitchell, R. H.; Moore, T. A.; Moore, A. L.; Gust, D. Molecular 2:1 Digital Multiplexer. *Angew. Chem., Int. Ed.* 2007, *46*, 958–961.
- (27) Straight, S. D.; Andréasson, J.; Kodis, G.; Bandyopadhyay, S.; Mitchell, R. H.; Moore, T. A.; Moore, A. L.; Gust, D. Molecular AND and INHIBIT Gates Based on Control of Porphyrin Fluorescence by Photochromes. *J. Am. Chem. Soc.* 2005, *127*, 9403–9409.
- (28) Roldan, D.; Cobo, S.; Lafolet, F.; Vilà, N.; Bochot, C.; Bucher, C.; Saint-Aman, E.; Boggio-Pasqua, M.; Garavelli, M.; Royal, G. A Multi-Addressable Switch Based on the Dimethyldihydropyrene Photochrome with Remarkable Proton-Triggered Photo-opening Efficiency. *Chem. – Eur. J.* 2015, *21*, 455–467.
- (29) Bakkar, A.; Cobo, S.; Lafolet, F.; Saint-Aman, E.; Royal, G. A new surface-bound molecular switch based on the photochromic dimethyldihydropyrene with light-driven release of singlet oxygen properties. *J. Mater. Chem. C* 2015, *3*, 12014–12017.
- (30) Wang, Q.; Ligorio, G.; Schlesinger, R.; Diez-Cabanes, V.; Cornil, D.; Garmshausen, Y.; Hecht, S.; Cornil, J.; List-Kratochvil, E. J. W.; Koch, N. Switching the Electronic Properties of ZnO Surfaces with Negative T-Type Photochromic Pyridyl-dihydropyrene Layers and Impact of Fermi Level Pinning. *Adv. Mater. Interfaces* 2019, *6*, No. 1900211.
- (31) Ayub, K.; Mitchell, R. H. Syntheses of dihydropyrene-cyclophanediene negative photochromes containing internal alkenyl and alkynyl groups and comparison of their photochemical and thermochemical properties. *J. Org. Chem.* 2014, *79*, 664–678.
- (32) Boekelheide, V.; Sturm, E. Aromatic molecules bearing substituents within the cavity of the π -electron cloud. Optical resolution and thermal rearrangement studies. *J. Am. Chem. Soc.* 1969, *91*, 902–908.
- (33) Kimball, D. B.; Haley, M. M.; Mitchell, R. H.; Ward, T. R.; Bandyopadhyay, S.; Williams, R. V.; Armantrout, J. R. Dimethyldihydropyrene–Dehydrobenzoannulene Hybrids: Studies in Aromaticity and Photoisomerization. *J. Org. Chem.* 2002, *67*, 8798–8811.
- (34) Mitchell, R. H. The Metacyclophanediene-Dihydropyrene Photochromic π Switch. *Eur. J. Org. Chem.* 1999, *1999*, 2695–2703.
- (35) Mitchell, R. H.; Brkic, Z.; Sauro, V. A.; Berg, D. J. A Photochromic, Electrochromic, Thermochromic Ru Complexed Benzannulene: an Organometallic Example of the Dimethyldihydropyrene-Metacyclophanediene Valence Isomerization. *J. Am. Chem. Soc.* 2003, *125*, 7581–7585.
- (36) Mitchell, R. H.; Ward, T. R. The synthesis of benz-, naphth-, and anth-annulated dihydropyrenes as aids to measuring aromaticity by NMR. *Tetrahedron* 2001, *57*, 3689–3695.
- (37) Tashiro, M.; Yamato, T. Metacyclophanes and related compounds. 5. Thermal rearrangement of 10b,10c-dialkyl-2,7-ditert-butyl-trans-10b,10c-dihydropyrenes. *J. Org. Chem.* 1982, *47*, 2783–2785.
- (38) Mitchell, R. H.; Zhang, L. M. Synthesis, reactions, and structural and NMR features of [2.2]metacyclophane monoenes and their tricarbonylchromium and cyclopentadienyliron(+) complexes. *J. Org. Chem.* 1999, *64*, 7140–7152.
- (39) Mitchell, R. H.; Chen, Y.; Khalifa, N.; Zhou, P. The Synthesis, Aromaticity, and NMR Properties of [14]Annulene Fused Organometallics. Determination of the Effective Bond Localizing Ability (“Relative Aromaticity”) and Diamagnetic Anisotropy of Several Organometallic Moieties. *J. Am. Chem. Soc.* 1998, *120*, 1785–1794.
- (40) Mitchell, R. H.; Ward, T. R.; Chen, Y.; Wang, Y.; Weerawarna, S. A.; Dibble, P. W.; Marsella, M. J.; Almutairi, A.; Wang, Z.-Q. Synthesis and Photochromic Properties of Molecules Containing [e]-Annulated Dihydropyrenes. Two and Three Way π -Switches Based on the Dimethyldihydropyrene–Metacyclophanediene Valence Isomerization. *J. Am. Chem. Soc.* 2003, *125*, 2974–2988.
- (41) Boekelheide, V.; Hylton, T. A. Aromatic molecules bearing substituents within the cavity of the π -electron cloud. General method for the synthesis of trans-15,16-dialkyldihydropyrenes. *J. Am. Chem. Soc.* 1970, *92*, 3669–3675.
- (42) Boekelheide, V.; Miyasaka, T. Aromatic Molecules Bearing Substituents within the Cavity of the π -Electron Cloud. Synthesis of trans-15,16-Diethyldihydropyrene. *J. Am. Chem. Soc.* 1967, *89*, 1709–1714.
- (43) Renfroe, H. B.; Gurney, J. A.; Hall, L. A. R. Synthesis and chemistry of hexamethyl-trans-15,16-dihydropyrene. *J. Org. Chem.* 1972, *37*, 3045–3052.
- (44) Al-Owaidi, O. A.; Bock, S.; Milan, D. C.; Oerthel, M.-C.; Inkpen, M. S.; Yufit, D. S.; Sobolev, A. N.; Long, N. J.; Albrecht, T.; Higgins, S. J.; Bryce, M. R.; Nichols, R. J.; Lambert, C. J.; Low, P. J. Insulated molecular wires: inhibiting orthogonal contacts in metal complex based molecular junctions. *Nanoscale* 2017, *9*, 9902–9912.

- (45) Kiguchi, M.; Nakashima, S.; Tada, T.; Watanabe, S.; Tsuda, S.; Tsuji, Y.; Terao, J. Single-Molecule Conductance of π -Conjugated Rotaxane: New Method for Measuring Stipulated Electric Conductance of π -Conjugated Molecular Wire Using STM Break Junction. *Small* 2012, 8, 726–730.
- (46) Lin, W. Preparation of Polyfunctionalised Grignard Reagents and their Application in Aryne Chemistry, Dissertation; Ludwig-Maximilians-Universität München: Munich, 2006.
- (47) Kersting, B.; DeLion, M. Synthesis of Benzisochalcogenol and -azole Derivatives via ortho Metalation of Isophthalamides. *Z. Naturforsch. B* 1999, 54, 1042–1047.
- (48) Kristensen, J.; Lysén, M.; Vedsø, P.; Begtrup, M. Synthesis of Ortho Substituted Arylboronic Esters by in Situ Trapping of Unstable Lithio Intermediates. *Org. Lett.* 2001, 3, 1435–1437.
- (49) Armstrong, D. R.; Mulvey, R. E.; Barr, D.; Snaith, R.; Reed, D. Isolation, characterisation, and solution structures of the bis(pyridine) complex of the n-butyllithium-pyridine adduct, $\text{Bu}^n(\text{C}_5\text{H}_5\text{N})\text{Li}\cdot 2\text{C}_5\text{H}_5\text{N}$, its mode of decomposition, and ab initio calculations on model systems. *J. Organomet. Chem.* 1988, 350, 191–205.
- (50) Richey, H. G.; Farkas, J. Reactions of dialkylmagnesium-organolithium solutions with pyridine, quinoline, and cyclohexenone. *Organometallics* 1990, 9, 1778–1784.
- (51) Kloss, F.; Krchnak, V.; Krchnakova, A.; Schieferdecker, S.; Dreisbach, J.; Krone, V.; Möllmann, U.; Hoelscher, M.; Miller, M. J. In Vivo Dearomatization of the Potent Antituberculosis Agent BTZ043 via Meisenheimer Complex Formation. *Angew. Chem., Int. Ed.* 2017, 56, 2187–2191.
- (52) Young, W. B.; Barbosa, J.; Blomgren, P.; Bremer, M. C.; Crawford, J. J.; Dambach, D.; Eigenbrot, C.; Gallion, S.; Johnson, A. R.; Kropf, J. E.; Lee, S. H.; Liu, L.; Lubach, J. W.; Macaluso, J.; Maciejewski, P.; Mitchell, S. A.; Ortwine, D. F.; Di Paolo, J.; Reif, K.; Scheerens, H.; Schmitt, A.; Wang, X.; Wong, H.; Xiong, J.-M.; Xu, J.; Yu, C.; Zhao, Z.; Currie, K. S. Discovery of highly potent and selective Bruton's tyrosine kinase inhibitors: Pyridazinone analogs with improved metabolic stability. *Bioorg. Med. Chem. Lett.* 2016, 26, 575–579.
- (53) Lamont, S. G.; Donald, C. S.; Lyman Feron, J.; Groombridge, S. D. Regioselective ortho alkylation of nitro indole, carbazole, benzothiophene and benzofuran. *Tetrahedron Lett.* 2015, 56, 7165–7167.
- (54) Niu, C.; Boschelli, D. H.; Tumey, L. N.; Bhagirath, N.; Subrath, J.; Shim, J.; Wang, Y.; Wu, B.; Eid, C.; Lee, J.; Yang, X.; Brennan, A.; Chaudhary, D. First generation 5-vinyl-3-pyridinecarbonitrile PKC θ inhibitors. *Bioorg. Med. Chem. Lett.* 2009, 19, 5829–5832.
- (55) Noguchi, T.; Tanaka, N.; Nishimata, T.; Goto, R.; Hayakawa, M.; Sugidachi, A.; Ogawa, T.; Asai, F.; Ozeki, T.; Fujimoto, K. Indoline Derivatives II: Synthesis and Factor χ_a (FXa) Inhibitory Activities. *Chem. Pharm. Bull.* 2007, 55, 393–402.
- (56) Małosza, M.; Varvounis, G.; Surowiec, M.; Giannopoulou, T. Tele vs. Oxidative Substitution of Hydrogen in meta Monochloromethyl, Dichloromethyl, and Trichloromethyl Nitrobenzenes in the Reaction with Grignard Reagents. *Eur. J. Org. Chem.* 2003, 2003, 3791–3797.
- (57) Matveev, M. R.; Ponyaev, A. I.; El'tsov, A. V. Photochromic Properties of ortho-Methylnitrobenzothiazoles in Solution. *Russ. J. Gen. Chem.* 2001, 71, 1286–1292.
- (58) Mitchell, R. H.; Zhang, J. A new synthesis of thiacyclophanes from thiolacetates. *Tetrahedron Lett.* 1995, 36, 1177–1180.
- (59) Tashiro, M.; Yamato, T. Metacyclophanes and Related Compounds. 4. Halogenations of 8,16-Dialkyl-anti-5,13-di-tert-butyl[2.2]metacyclophan-1-enes and 2,7-Di-tert-butyl-trans-10b,10c-dialkyl-10b,10c-dihydropyrenes. *J. Am. Chem. Soc.* 1982, 104, 3701–3707.
- (60) Mitchell, R. H.; Vinod, T. K.; Bushnell, G. W. syn-[2.2]Metacyclophane: Isolation, NMR Properties, and Facile Isomerization to anti-[2.2]Metacyclophane. A Synthesis Involving Bridge Reactions of Chromium Tricarbonyl Complexed Dithiametacyclophanes. *J. Am. Chem. Soc.* 1990, 112, 3487–3497.
- (61) Ting, Y.; Lai, Y.-H. Extreme Projection of a Proton into the π -Cloud of an Aromatic Ring: Record Shielding of an Aromatic Proton in trans-10b-Methyl-10c-(1-naphthyl)-10b,10c-dihydropyrene. *J. Am. Chem. Soc.* 2004, 126, 909–914.
- (62) Chifuku, K.; Sawada, T.; Kuwahara, Y.; Shosenji, H. The Synthesis and Property of Dihydropyrene Derivatives Containing a Nitrogen Atom. *Mol. Cryst. Liq. Cryst.* 2007, 470, 369–381.
- (63) Lai, Y.-H.; Eu, H.-L. Novel Formation of 4-Methylthiopyrene in a Hofmann Elimination Reaction Directed Toward the Synthesis of 17,19-Dioxa[2.2.3](1,2,3)cyclophanediene. *J. Chem. Soc., Perkin Trans. 1* 1993, 233–237.
- (64) Davy, J. R.; Iskander, M. N.; Reiss, J. A. [2.2] (2,7)-Naphthalenoparacyclophanes. *Tetrahedron Lett.* 1978, 19, 4085–4088.
- (65) Davy, J. R.; Iskander, M. N.; Reiss, J. A. Approaches to the Synthesis of Corannulene. *Aust. J. Chem.* 1979, 32, 1067–1078.
- (66) Ayub, K.; Li, R.; Bohne, C.; Williams, R. V.; Mitchell, R. H. Calculation Driven Synthesis of an Excellent Dihydropyrene Negative Photochrome and its Photochemical Properties. *J. Am. Chem. Soc.* 2011, 133, 4040–4045.
- (67) Roemer, M.; Gillespie, A. A.; Turner, G. F.; Flematti, G. R.; Hobday, C. L.; Sobolev, A. N.; Wild, D. A.; Nealon, G. L.; Piggott, M. J.; Moggach, S. A.; Koutsantonis, G. A. A Merry Dance Across the π -Cloud: Tracking the Transformation of a 2,7-Substituted Dihydropyrene Through a Thermally Stimulated Single-Crystal-to-Single-Crystal Reaction. *Cryst. Growth Des.* 2021, 21, 6558–6566.
- (68) Hong, W.; Manrique, D. Z.; Moreno-García, P.; Gulcur, M.; Mishchenko, A.; Lambert, C. J.; Bryce, M. R.; Wandlowski, T. Single molecular conductance of tolanes: Experimental and theoretical study on the junction evolution dependent on the anchoring group. *J. Am. Chem. Soc.* 2012, 134, 2292–2304.
- (69) Lu, Q.; Kole, G. K.; Friedrich, A.; Müller-Buschbaum, K.; Liu, Z.; Yu, X.; Marder, T. B. Comparison Study of the Site-Effect on Regioisomeric Pyridyl–Pyrene Conjugates: Synthesis, Structures, and Photophysical Properties. *J. Org. Chem.* 2020, 85, 4256–4266.
- (70) Canton, M.; Grommet, A. B.; Pesce, L.; Gemen, J.; Li, S.; Diskin-Posner, Y.; Credi, A.; Pavan, G. M.; Andréasson, J.; Klajn, R. Improving Fatigue Resistance of Dihydropyrene by Encapsulation within a Coordination Cage. *J. Am. Chem. Soc.* 2020, 142, 14557–14565.
- (71) Liddell, P. A.; Kodis, G.; Andréasson, J.; de la Garza, L.; Bandyopadhyay, S.; Mitchell, R. H.; Moore, T. A.; Moore, A. L.; Gust, D. Photonic Switching of Photoinduced Electron Transfer in a Dihydropyrene–Porphyrin–Fullerene Molecular Triad. *J. Am. Chem. Soc.* 2004, 126, 4803–4811.
- (72) Muratsugu, S.; Nishihara, H. π -Conjugation modification of photochromic and redox-active dimethyldihydropyrene by phenyl- and ethynyl-terpyridines and Ru(bis-terpyridine) complexes. *New J. Chem.* 2014, 38, 6114–6124.
- (73) Lozeman, J. J. A.; Führer, P.; Olthuis, W.; Odijk, M. Spectroelectrochemistry, the future of visualizing electrode processes by hyphenating electrochemistry with spectroscopic techniques. *Analyst* 2020, 145, 2482–2509.
- (74) Zhai, Y.; Zhu, Z.; Zhou, S.; Zhu, C.; Dong, S. Recent advances in spectroelectrochemistry. *Nanoscale* 2018, 10, 3089–3111.
- (75) Sheepwash, M. A. L.; Mitchell, R. H.; Bohne, C. Mechanistic insights into the photochromism of trans-10b, 10c-dimethyl-10b, 10c-dihydropyrene derivatives. *J. Am. Chem. Soc.* 2002, 124, 4693–4700.
- (76) Sheepwash, M. A. L.; Ward, T. R.; Wang, Y.; Bandyopadhyay, S.; Mitchell, R. H.; Bohne, C. Mechanistic studies on the photochromism of [e]-annelated dimethyldihydropyrenes. *Photochem. Photobiol. Sci.* 2003, 2, 104–112.
- (77) Kishida, M.-a.; Kusamoto, T.; Nishihara, H. Photoelectric Signal Conversion by Combination of Electron-Transfer Chain Catalytic Isomerization and Photoisomerization on Benzodimethyldihydropyrenes. *J. Am. Chem. Soc.* 2014, 136, 4809–4812.
- (78) Bakkar, A.; Lafolet, F.; Boggio-Pasqua, M.; Jouvenot, D.; Saint-Aman, E.; Cobo, S. Electrochemical control of the switching process

of photochromic dimethyldihydropyrene derivatives. *Chem. Commun.* 2017, 53, 9360–9363.

(79) Connelly, N. G.; Geiger, W. E. Chemical Redox Agents for Organometallic Chemistry. *Chem. Rev.* 1996, 96, 877–910.

(80) Xu, B.; Tao, N. J. Measurement of Single-Molecule Resistance by Repeated Formation of Molecular Junctions. *Science* 2003, 301, 1221–1223.

(81) Mitchell, R. H.; Bandyopadhyay, S. Linked photoswitches where both photochromes open and close. *Org. Lett.* 2004, 6, 1729–1732.

(82) Kishida, M.-a.; Muratsugu, S.; Sakamoto, R.; Kusamoto, T.; Nishihara, H. Efficient Electronic Communication in 4,9-Bis-(ferrocenylethynyl)dimethyldihydropyrene. *Chem. Lett.* 2013, 42, 361–362.

(83) Ghosh, S.; Hossain, M. S.; Chatterjee, S.; Rahaman, S. A.; Bandyopadhyay, S. Light-Gated Modulation of Electronic Mobility of a Dihydropyrene-Based Photochromic Coordination Polymer. *ACS Appl. Mater. Interfaces* 2020, 12, 52983–52991.

(84) Tsuji, Y.; Hoffmann, R. Frontier Orbital Control of Molecular Conductance and its Switching. *Angew. Chem., Int. Ed.* 2014, 53, 4093–4097.

(85) Naghibi, S.; Ismael, A. K.; Vezzoli, A.; Al-Khaykane, M. K.; Zheng, X.; Grace, I. M.; Bethell, D.; Higgins, S. J.; Lambert, C. J.; Nichols, R. J. Synthetic Control of Quantum Interference by Regulating Charge on a Single Atom in Heteroaromatic Molecular Junctions. *J. Phys. Chem. Lett.* 2019, 10, 6419–6424.

(86) Aradhya, S. V.; Meisner, J. S.; Krikorian, M.; Ahn, S.; Parameswaran, R.; Steigerwald, M. L.; Nuckolls, C.; Venkataraman, L. Dissecting Contact Mechanics from Quantum Interference in Single-Molecule Junctions of Stilbene Derivatives. *Nano Lett.* 2012, 12, 1643–1647.

(87) Arroyo, C. R.; Tarkuc, S.; Frisenda, R.; Seldenthuis, J. S.; Woerde, C. H. M.; Eelkema, R.; Grozema, F. C.; van der Zant, H. S. J. Signatures of Quantum Interference Effects on Charge Transport Through a Single Benzene Ring. *Angew. Chem., Int. Ed.* 2013, 52, 3152–3155.

(88) Xu, B. Q.; Dubi, Y. Negative differential conductance in molecular junctions: an overview of experiment and theory. *J. Phys.: Condens. Matter* 2015, 27, No. 263202.

(89) Wu, C.; Qiao, X.; Robertson, C. M.; Higgins, S. J.; Cai, C.; Nichols, R. J.; Vezzoli, A. A Chemically Soldered Polyoxometalate Single-Molecule Transistor. *Angew. Chem., Int. Ed.* 2020, 59, 12029–12034.

(90) Olavarria-Contreras, I. J.; Etcheverry-Berrios, A.; Qian, W.; Gutiérrez-Cerón, C.; Campos-Olguín, A.; Sañudo, E. C.; Dulic, D.; Ruiz, E.; Aliaga-Alcalde, N.; Soler, M.; van der Zant, H. S. J. Electric-field induced bistability in single-molecule conductance measurements for boron coordinated curcuminoid compounds. *Chem. Sci.* 2018, 9, 6988–6996.

(91) Zhang, L.; Laborda, E.; Darwish, N.; Noble, B. B.; Tyrell, J. H.; Pluczyk, S.; Le Brun, A. P.; Wallace, G. G.; Gonzalez, J.; Coote, M. L.; Ciampi, S. Electrochemical and Electrostatic Cleavage of Alkoxyamines. *J. Am. Chem. Soc.* 2018, 140, 766–774.

(92) Shaik, S.; de Visser, S. P.; Kumar, D. External Electric Field Will Control the Selectivity of Enzymatic-Like Bond Activations. *J. Am. Chem. Soc.* 2004, 126, 11746–11749.

(93) Aragones, A. C.; Haworth, N. L.; Darwish, N.; Ciampi, S.; Bloomfield, N. J.; Wallace, G. G.; Diez-Perez, I.; Coote, M. L. Electrostatic catalysis of a Diels-Alder reaction. *Nature* 2016, 531, 88–91.

(94) Evangeli, C.; Gillemot, K.; Leary, E.; González, M. T.; Rubio-Bollinger, G.; Lambert, C. J.; Agraït, N. Engineering the Thermopower of C₆₀ Molecular Junctions. *Nano Lett.* 2013, 13, 2141–2145.

(95) Rincón-García, L.; Evangeli, C.; Rubio-Bollinger, G.; Agraït, N. Thermopower measurements in molecular junctions. *Chem. Soc. Rev.* 2016, 45, 4285–4306.

(96) Widawsky, J. R.; Darancet, P.; Neaton, J. B.; Venkataraman, L. Simultaneous Determination of Conductance and Thermopower of Single Molecule Junctions. *Nano Lett.* 2012, 12, 354–358.

(97) Quek, S. Y.; Kamenetska, M.; Steigerwald, M. L.; Choi, H. J.; Louie, S. G.; Hybertsen, M. S.; Neaton, J. B.; Venkataraman, L. Mechanically controlled binary conductance switching of a single-molecule junction. *Nat. Nanotechnol.* 2009, 4, 230–234.

(98) Yanson, A. I.; Bollinger, G. R.; van den Brom, H. E.; Agraït, N.; van Ruitenbeek, J. M. Formation and manipulation of a metallic wire of single gold atoms. *Nature* 1998, 395, 783–785.

(99) Soler, J. M.; Artacho, E.; Gale, J. D.; García, A.; Junquera, J.; Ordejón, P.; Sánchez-Portal, D. The SIESTA method for ab initio order-N materials simulation. *J. Phys.: Condens. Matter* 2002, 14, 2745–2779.

(100) Lambert, C. J. *Quantum Transport in Nanostructures and Molecules*, IOP Publishing, 2021.

(101) Sadeghi, H. Theory of electron, phonon and spin transport in nanoscale quantum devices. *Nanotechnology* 2018, 29, No. 373001.

(102) Dolomanov, O. V.; Bourhis, L. J.; Gildea, R. J.; Howard, J. A. K.; Puschmann, H. OLEX2: a complete structure solution, refinement and analysis program. *J. Appl. Crystallogr.* 2009, 42, 339–341.